CHARACTERIZATION OF UBIQUITIN LIGASE TARGETING

BY ANTICANCER SULFONAMIDES

APPROVED BY SUPERVISORY COMMITTEE:

Deepak Nijhawan, M.D., Ph.D.

George DeMartino, Ph.D.

Hongtao Yu, Ph.D.

Russell DeBose-Boyd, Ph.D.

DEDICATION

To my wonderful mother

“There are some who bring a light so great to the world that even after they have gone, the light remains.” -*Anon.*

CHARACTERIZATION OF UBIQUITIN LIGASE TARGETING BY ANTICANCER SULFONAMIDES

by

TABITHA C. TING

DISSERTATION

Presented to the Faculty of the Graduate School of Biomedical Sciences

The University of Texas Southwestern Medical Center at Dallas

In Partial Fulfillment of the Requirements

For the Degree of

DOCTOR OF PHILOSOPHY

The University of Texas Southwestern Medical Center at Dallas

Dallas, Texas

August 2020

ACKNOWLEDGEMENTS

This work would not have been possible without the support and contributions of many people. First, I would like to acknowledge and thank my mentor, Deepak Nijhawan, for accepting me as a student and allowing me to pursue these projects in his lab. I also thank my dissertation committee members Dr. George DeMartino, Dr. Hongtao Yu, and Dr. Russell DeBose-Boyd for their encouragement and expertise during these past few years of Ph.D. training. I would also like to thank my past mentor, Dr. Makoto Miyazaki, for instilling the love of science in me as I would not have continued without that spark. The insights and advice of these faculty were invaluable to my training, and I am deeply grateful for their mentorship.

I cannot express enough gratitude to two past members of the lab, Nicholas Gaskill and Ting Han. My only request as a student was to learn how to do science, and they both illuminated the path toward that goal. Although we only worked together for a few months, I have never learned more during my graduate school education than I did during that brief time. I would also like to thank Maria Goralski for her relentlessly hard work throughout this project. She restored my faith that there are people who care about the quality of their work, and I have no doubt that she will be immensely successful in her next chapter of life. I also thank Baiyun Wang for her work on several of the *in vitro* binding assays outlined in this thesis. It has been a pleasure to collaborate with her on this project and others.

Thank you to the many friends who have listened and supported me throughout the past few years. Their friendships have been my lifeline, and I am honored to have known each and every one of them. And last but certainly not least, I would like to thank my father,

Dr. Albert Ting. As I grow older, I have developed a greater appreciation of what a rare and truly wonderful person he is, and I thank him for his unconditional love and support, regardless of the outcome.

CHARACTERIZATION OF UBIQUITIN LIGASE TARGETING

BY ANTICANCER SULFONAMIDES

Tabitha C. Ting, Ph.D.

The University of Texas Southwestern Medical Center at Dallas, 2020

Supervising Professor: Deepak Nijhawan, M.D., Ph.D.

Aryl sulfonamides are small molecules that are selectively toxic to a subset of human cancer cell lines. Clinical trials of the aryl sulfonamide indisulam have resulted in modest clinical activity against a subset of solid tumors. Recent work revealed that indisulam recruits the RNA binding protein RBM39 to DCAF15, a component of the CRL4-DCAF15 E3 ubiquitin ligase. This recruitment results in RBM39 ubiquitination and degradation, leading to splicing defects and cancer cell death (Han et al., 2017; Uehara et al., 2017). The mechanism of action of sulfonamides is similar to that of immunomodulatory drugs (IMiDs), which recruit substrates to the closely related CRL4-CRBN E3 ubiquitin ligase for ubiquitination. Known for their roles in inhibiting embryonic development and cancer cell

growth, IMiDs exert their pleiotropic effects by targeting a variety of substrate proteins to the CRL4-CRBN E3. Despite major advances in our understanding of aryl sulfonamides, it is unclear whether sulfonamides also target multiple substrates or modulate the endogenous function of the CRL4-DCAF15 E3 ligase. This dissertation describes our efforts to define the requirements for RBM39 ubiquitination, identify other substrates that are recruited to the CRL4-DCAF15 E3 ligase, and further our understanding of the cellular consequences of indisulam treatment. In Chapters 2 and 3, we define the components required for RBM39 ubiquitination using a combination of *in vitro* and *in vivo* techniques. In Chapters 4 and 5, we identify putative endogenous substrates and a previously undescribed neo-substrate recruited to the CRL4-DCAF15 E3 ligase for ubiquitination. We also generate a mouse model to explore the physiologic role of DCAF15. In Chapter 6, we characterize the cellular consequences of indisulam treatment and neo-substrate degradation. In aggregate, this work aims to contribute to our understanding of the aryl sulfonamide mechanism of action and the field of targeted protein degradation.

TABLE OF CONTENTS

PRIOR PUBLICATIONS

1. Ting, T.C., Goralski, M., Klein, K., Wang, B., Kim, J., Xie, Y., and Nijhawan, D. (2019). Aryl Sulfonamides Degrade RBM39 and RBM23 by Recruitment to CRL4-DCAF15. Cell Rep 29, 1499-1510.
2. Fernandez, A.F., Sebti, S., Wei, Y., Zou, Z., Shi, M., McMillan, K.L., He, C., Ting, T.C., Liu, Y., Chiang, W.C., et al. (2018). Disruption of the Beclin 1-BCL2 autophagy regulatory complex promotes longevity in mice. Nature 558, 136-140.
3. Han, T., Goralski, M., Gaskill, N., Capota, E., Kim, J., Ting, T.C., Xie, Y., Williams, N.S., and Nijhawan, D. (2017). Anticancer sulfonamides target splicing by inducing RBM39 degradation via recruitment to DCAF15. Science 356.
4. Rocchi, A., Yamamoto, S., Ting, T.C., Fan, Y., Sadleir, K., Wang, Y., Zhang, W., Huang, S., Levine, B., Vassar, R., et al. (2017). A Becn1 mutation mediates hyperactive autophagic sequestration of amyloid oligomers and improved cognition in Alzheimer's disease. PLoS Genet 13, e1006962.
5. Masuda, M., Miyazaki-Anzai, S., Levi, M., Ting, T.C., and Miyazaki, M. (2013). PERK-eIF2α-ATF4-CHOP signaling contributes to TNFα-induced vascular calcification. J Am Heart Assoc 2, e000238.
6. Ting, T.C., and Miyazaki, M. (2013). "Stearoyl-CoA Desaturase-1 in the Regulation of Toll-Like Receptor Signaling and Endoplasmic Reticulum Stress Signaling." In *Stearoyl-CoA Desaturase Genes in Lipid Metabolism.* Springer Science and Business Media, New York, NY, pp. 73–84. https://doi.org/10.1007/978-1-4614-7969-7.

7. Masuda, M., Ting, T.C., Levi, M., Saunders, S.J., Miyazaki-Anzai, S., and Miyazaki, M. (2012). Activating transcription factor 4 regulates stearate-induced vascular calcification. J Lipid Res 53, 1543-1552.
8. Ting, T.C., Miyazaki-Anzai, S., Masuda, M., Levi, M., Demer, L.L., Tintut, Y., and Miyazaki, M. (2011). Increased lipogenesis and stearate accelerate vascular calcification in calcifying vascular cells. J Biol Chem *286*, 23938-23949.
9. Geng, Y., Hsu, J.J., Lu, J., Ting, T.C., Miyazaki, M., Demer, L.L., and Tintut, Y. (2011). Role of cellular cholesterol metabolism in vascular cell calcification. J Biol Chem 286, 33701-33706.
10. Miyazaki-Anzai, S., Levi, M., Kratzer, A., Ting, T.C., Lewis, L.B., and Miyazaki, M. (2010). Farnesoid X receptor activation prevents the development of vascular calcification in ApoE-/- mice with chronic kidney disease. Circ Res 106, 1807-1817.

LIST OF FIGURES

LIST OF TABLES

LIST OF ABBREVIATIONS

AID - Auxin-Inducible Degron

BCR-ABL - Breakpoint Cluster Region-Abelson

CAR - Chimeric Antigen Receptor

CK1α - Casein Kinase 1 Alpha

CRBN - Cereblon

CRL - Cullin-RING Ubiquitin Ligase

CQS - Chloroquinoxaline sulfonamide

DCAF15 - DDB1 And CUL4 Associated Factor 15

DDA1 - DET1 And DDB1 Associated 1

DDB1 - Damage-Specific DNA Binding Protein 1

GSPT1 - G to S phase transition protein-1

HRP - Horseradish peroxidase

IKZF1 - IKAROS Family Zinc Finger 1 (Ikaros)

IKZF3 - IKAROS family zinc finger 3 (Aiolos)

IMID - Immunomodulatory Drug

RBM23- RNA Binding Motif Protein 23

RBM39 - RNA Binding Motif Protein 39

RBP - RNA Binding Protein

RBX1 - RING Box Protein 1

RRM - RNA Recognition Motif

SALL4 - Sal-like protein 4

SILAC - Stable Isotope Labeling by Amino acids in Culture

TIR1 - Transport Inhibitor Response 1

TR-FRET - Time-Resolved Fluorescence Energy Transfer

CHAPTER ONE: INTRODUCTION

Challenges in Cancer Drug Discovery

For many years, the mainstay of cancer treatment consisted of nonspecific modalities such as cytotoxic chemotherapy or radiation. Many of these early chemotherapeutic drugs targeted DNA, microtubules and other cellular components common in many types of normal tissues in addition to cancer cells. However, recent approaches in cancer drug discovery have focused on developing inhibitors of specific cancer drivers. Early in the targeted therapy revolution was the development of treatments like imatinib, which inhibits the tyrosine kinase activity of the BCR-ABL fusion protein in chronic myeloid leukemia (Druker et al., 1996; Groffen et al., 1984; Heisterkamp et al., 1983; Lugo et al., 1990; Peng et al., 2004; Rowley, 1973). One of the most recent groundbreaking advances in cancer therapy is in the field of immunotherapy. Development of immune checkpoint inhibitors, chimeric antigen receptor (CAR) T cells, and oncolytic viruses has harnessed the immune system to target cancer cells (Andtbacka et al., 2015; Brunet et al., 1987; Eshhar et al., 1993; Hodi et al., 2010; Kaplan et al., 1998; Krummel and Allison, 1995; Leach et al., 1996; Ribas et al., 2017; Shankaran et al., 2001). These treatments have revolutionized clinical oncology and provided a wider range of therapeutic options.

Despite the advent of novel strategies like immunotherapy, discovery of anti-cancer drugs is still a crucial area of research. Currently, most therapies are small molecules or antibodies that exert their effects by modulating the function of proteins such as enzymes,

receptors, or transporters. Many of these drugs occupy a binding pocket or active site to inhibit protein function. However, tumor cells often develop resistance to these small molecules through multiple heterogeneous mechanisms, leading to the need for development of alternative therapies. In addition, many of these drugs have undesirable off-target effects due to structural similarities between their target proteins and other related proteins. For example, many kinase inhibitors are well known for targeting a wide range of kinases with similar binding pockets, resulting in many off-target side effects (Hanson et al., 2019; Karaman et al., 2008; Klaeger et al., 2017).

The number of anti-cancer drugs and their protein targets is limited, even with current advances in targeted therapy. Out of the thousands of proteins encoded by the human genome, it is estimated that FDA-approved cancer therapies target fewer than 800 of these proteins (Che et al., 2018; Overington et al., 2006; Rask-Andersen et al., 2011; Santos et al., 2017). Many putative drivers of tumorigenesis have been discovered through recent cancer research and The Cancer Genome Atlas (TCGA) program, which provides sequencing data on thousands of patient samples. Although these studies have identified a large number of targets, a major challenge in cancer drug development is the difficulty of targeting proteins that lack receptor or enzymatic sites, and therefore do not present binding pockets that can be utilized for small molecule design (Dang et al., 2017). These proteins are often labeled as "undruggable," and include transcription factors, scaffolding proteins, and pseudokinases (Dang et al., 2017; Huang and Dixit, 2016; Salami and Crews, 2017). Several key oncogenic drivers such as KRAS and MYC are among the many proteins that comprise this class of

currently undruggable targets. Overcoming this challenge will likely involve expansion of chemical space in order to target proteins through novel mechanisms.

Development of Molecular Glues for Cancer Therapy

A new class of pharmacotherapeutic molecules has recently emerged for targeting conventionally "undruggable" proteins. These compounds are referred to as molecular glues because they recruit a target protein to an E3 ubiquitin ligase receptor (Baek and Schulman, 2020; Che et al., 2018; Verma et al., 2020). These target proteins are known as neo-substrates because they are only recruited to the E3 ligase in the presence of a molecular glue. This recruitment results in the degradation of the protein target through the ubiquitin-proteasome pathway (Figure 1-1). In this pathway, a ubiquitin-activating enzyme (E1) forms a thioester bond with the C terminus of ubiquitin via an ATP-dependent reaction. Ubiquitin is then transferred to a ubiquitin-conjugating enzyme (E2), which associates with an E3 ubiquitin ligase. The largest class of E3s are the RING E3 ligases, which act as scaffolds to recruit substrate proteins and E2 enzymes. Cullin-RING ligases are comprised of a Cullin scaffolding protein, adaptors to recruit other E3 components, substrate receptors to bind the protein target, and RING-box proteins for recruiting E2 ubiquitin-conjugating enzymes. Inducing proximity among these proteins facilitates the transfer of ubiquitin onto substrate lysine residues. Subsequent ubiquitin addition leads to the formation of a polyubiquitin chain, which targets the substrate for degradation by the proteolytic activity of the multi-subunit proteasome.

A notable example of molecular glues that hijack the ubiquitin-proteasome system are the immunomodulatory drugs (IMiDs), which include thalidomide, lenalidomide, and pomalidomide. IMiDs bind the E3 ubiquitin ligase receptor cereblon (CRBN), and lead to the recruitment of a wide range of neo-substrates with broad cellular functions. For example, IMiDs are used to treat multiple myeloma by catalyzing the degradation of two transcription factors which contain zinc finger domains, Ikaros (IKZF1) and Aiolos (IKZF3) (Kronke et al., 2014; Lu et al., 2014). Another example of an IMiD substrate is the translation termination factor GSPT1, which is recruited to cereblon by the compound CC-885, leading to growth inhibition in acute myeloid leukemia cells. In addition to their effects on immune cell development and function, IMiDs also mediate degradation of another zinc finger domain-containing transcription factor, Sal-like protein 4 (SALL4), which leads to teratogenicity (Donovan et al., 2018; Matyskiela et al., 2018). IMiD derivatives demonstrate remarkable specificity for unique protein targets. For example, lenalidomide but not thalidomide induces degradation of casein kinase 1 alpha (CK1α), leading to clinical efficacy in the treatment of del(5q) myelodysplastic syndrome (Kronke et al., 2015).

Targeted protein degradation mediated by IMiDs and other molecular glues have introduced a new paradigm for the field of pharmacology. Historically, many drugs are small molecules that are required to remain bound to their protein target in order to achieve inhibition. Thus, a relatively high level of drug must be maintained, which may lead to undesirable off-target effects. In contrast, molecular glues are only required for a transient interaction between a protein target and the E3 ubiquitin ligase and do not need to remain bound to a single target, eliminating the need to maintain high levels of the drug. Thus,

molecular glues can be utilized for recruiting multiple targets for degradation with fewer off-target effects resulting from high concentrations (Lai and Crews, 2017). The specificity of these molecular glues for their protein targets also decreases their number of off-target effects, making them attractive therapeutic options.

In addition to molecular glues, proteolysis-targeting chimeras (PROTACs) are another class of molecules in the field of targeted protein degradation. PROTAC development applies knowledge about molecule glues towards the rational design of compounds that target novel proteins of interest (Rodriguez-Gonzalez et al., 2008; Sakamoto et al., 2001; Sakamoto et al., 2003; Schneekloth et al., 2004). PROTAC molecules are designed of three main components: 1) a ligand that recruits an E3 ubiquitin ligase, 2) a targeting ligand ("warhead") that can recruit the protein of interest, and 3) a chemical linker between the two ligands (Burslem et al., 2018; Fisher and Phillips, 2018; Hines et al., 2019; Lai et al., 2016; Paiva and Crews, 2019; Smith et al., 2019). By recruiting the desired protein of interest to an E3 ubiquitin ligase, PROTACs can mediate the ubiquitination and degradation of the chosen protein target. During initial development, these heterobifunctional molecules were large and bulky, leading to poor cell permeability and stability. However, later development led to PROTACs with improved drug-like properties. These include the small molecules ARV-110 and ARV-471, which are currently in clinical trials for prostate cancer and estrogen receptor positive breast cancer, respectively (Burslem and Crews, 2020; Mullard, 2019a, b).

Although PROTACs and molecular glues share a similar mechanism of action, these compounds have several key differences. First, PROTACs have affinities for both the E3

ligase and substrate, and therefore can bind each of these proteins independently. Because of this, a hook effect can occur where high PROTAC concentrations lead to binding of the molecule to either E3 ligase or substrate, but not to both (Bondeson et al., 2015; Douglass et al., 2013; Huang and Dixit, 2016; Pettersson and Crews, 2019). This lack of ternary complex formation leads to a loss in protein degradation with high PROTAC concentrations, which may contribute to pharmacological challenges regarding PROTAC dosing in patients. In contrast, many molecular glues do not possess a detectable affinity for free substrate (Chamberlain and Hamann, 2019; Han et al., 2017), and thus are not susceptible to the hook effect. Next, PROTACs are often bulky, high molecular weight molecules with undesirable properties including poor membrane permeability. Thus, extensive optimization of these molecules is often required to achieve adequate efficacy (Bondeson et al., 2015; Deshaies, 2015; Neklesa et al., 2017). In contrast, many of the discovered molecular glues are low molecular weight molecules that generally possess more favorable pharmacokinetic properties. This advantage of molecular glues may be due to the presence of additional contacts between the protein surfaces of the substrate and the E3 ligase, which help to stabilize the formation of the ternary complex (Bussiere et al., 2020; Matyskiela et al., 2020; Matyskiela et al., 2016; Petzold et al., 2016). Finally, the landscape of substrate targets for PROTACs and molecular glues has differed historically due to several factors. PROTAC development requires the extensive characterization of optimized binder molecules and their protein targets in order to design the “warhead” component of the molecule. Hence, many early PROTACs including those eventually placed in clinical trials were designed around well-defined molecules that bind established clinical targets such as the androgen receptor

(Mullard, 2019a, b; Rodriguez-Gonzalez et al., 2008; Salami et al., 2018). In contrast, the first discovered targets of several molecular glues included novel undruggable proteins such as transcription factors or RNA binding proteins. Prior to their discovery as molecular glue targets, many of these proteins had not been previously recognized as clinically relevant. Harnessing PROTAC technology to target more novel undruggable proteins still presents challenges that are currently being explored. For example, recent studies have reported heterobifunctional degraders for targeting aberrant tau in frontotemporal dementia models (Silva et al., 2019). Further studies will be required to discover additional molecular glues and develop more PROTACs for targeting the broad spectrum of undruggable proteins.

Identification of Molecular Glue Targets

Discovery of molecular glue targets often involves the identification of a degron, the minimal element of a protein substrate required for recruitment to the E3 ligase. For example, x-ray crystallography studies of CRBN in complex with an IMiD and different neo-substrates indicate that IMiDs recruit a common degron (Chamberlain et al., 2014; Fischer et al., 2014; Petzold et al., 2016) (Figure 1-2). The degron for IMiDs within IKZF1 and IKZF3 contains a conserved Cys_2-His_2 zinc finger motif (Petzold et al., 2016). Characterization of this structural degron led to the identification of eleven other IMiD-dependent substrates in a Cys_2-His_2 zinc finger library screen (Sievers et al., 2018).

Similar structural features in proteins without zinc finger domains can also serve as IMiD degrons. For example, the IMiD derivative CC-885 recruits the translation termination factor GSPT1, which has little homology to other known IMiD substrates except for a beta

hairpin containing a key glycine residue (Matyskiela et al., 2016). The fact that degrons may only possess similarities in structural motifs and not in primary sequence presents challenges for identifying other substrates. Currently, only a handful of molecular glues and substrates have been discovered. The ability of IMiD derivatives to target a wide range of proteins for degradation and their established clinical success provides a strong rationale for the development of molecular glues as therapy.

Discovery of the Aryl Sulfonamide Class of Molecular Glues

Recently, a second class of molecule glues was discovered by our lab and others (Han et al., 2017; Uehara et al., 2017). These compounds include indisulam and other structurally related aryl sulfonamides including tasisulam, E7820, and chloroquinoxaline sulfonamide (CQS) (Figure 1-3A). Indisulam was first discovered through phenotypic screens to selectively inhibit proliferation in a subset of human cancer cell lines (Fukuoka et al., 2001; Owa et al., 1999; Ozawa et al., 2001). Based on its anti-tumor activity in cell proliferation assays and tumor xenografts, indisulam was placed into clinical trials. In Phase I trials, indisulam was well-tolerated with no significant adverse side effects aside from myelosuppression (Dittrich et al., 2003; Terret et al., 2003; Yamada et al., 2005). However, several Phase II trials in multiple types of solid tumors demonstrated a low overall response rate (Haddad et al., 2004; Smyth et al., 2005; Talbot et al., 2007). Moreover, indisulam's mechanism of toxicity remained unclear for more than 15 years after its anti-tumor effects were reported. Due to insufficient knowledge on indisulam's mechanism of action, no biomarker was available for predicting patient responses to indisulam treatment.

Recently, our lab conducted a forward genetics screen to identify the target of indisulam. From this screen, mutations in the RNA recognition motif 2 (RRM2) domain of the splicing factor RBM39 were found to protect against indisulam toxicity in cell culture. From this study, we found that indisulam recruit the splicing factor RBM39 to the E3 ligase substrate receptor DCAF15. Recruitment of RBM39 to DCAF15 leads to RBM39 ubiquitination and degradation, which results in altered RNA splicing and death in a number of cancer cell lines (Figure 1-3B). Hematopoietic and lymphoid malignancies are more sensitive to indisulam cytotoxicity, highlighting the susceptibility of these cancers to splicing changes (Han et al., 2017). Likewise, a recent CRISPR-Cas9 screen demonstrated that RBM39 orchestrates a splicing program that is critical for the survival of acute myeloid leukemia cells (Wang et al., 2019).

RBM39 is the only known indisulam substrate. It is unclear whether sulfonamides like indisulam degrade a wide variety of substrates leading to differential cellular consequences. Many other RNA-binding proteins share homology with RBM39 and thus may also contain a degron that targets them for sulfonamide-dependent degradation. Here, we identify the degron within RBM39 as well as the residues in DCAF15 that are required for sulfonamide-dependent complex formation. Furthermore, we define the biochemical requirements for RBM39 recruitment and ubiquitination, and introduce RBM23 as another previously unreported neo-substrate of the CRL4-DCAF15 E3 ligase.

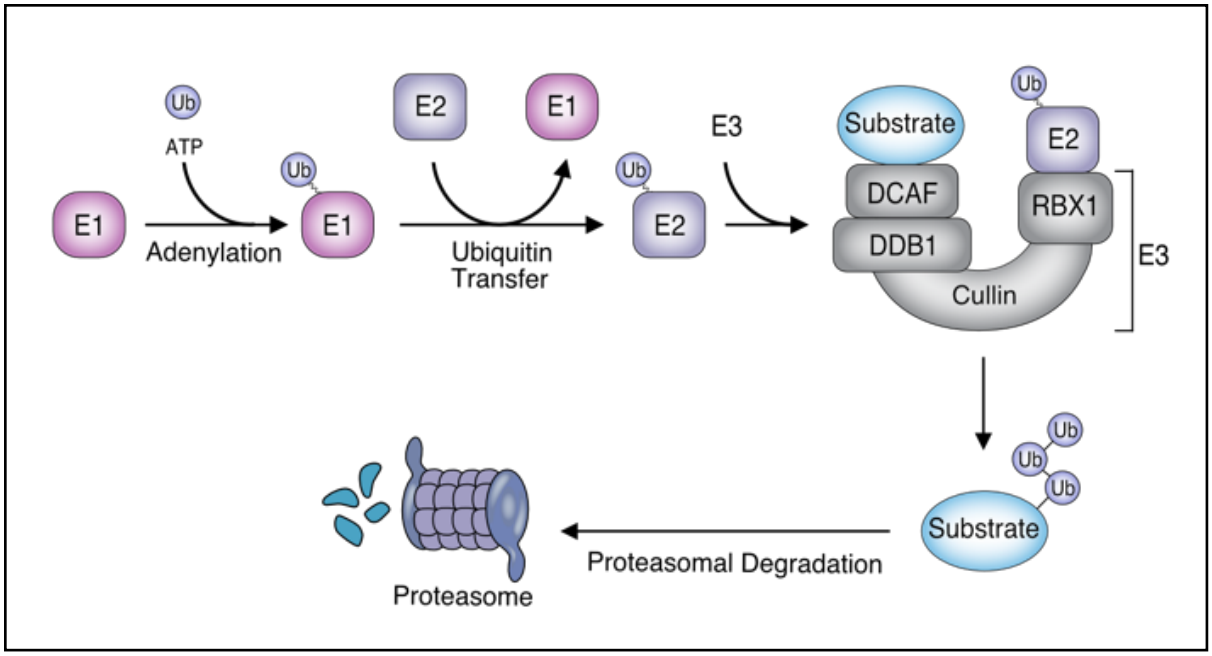

Figure 1-1. Ubiquitination cascade mediated by Cullin-RING E3 ligases.

The ubiquitination pathway is mediated by sets of specialized enzymes including ubiquitin-activating enzymes (E1), ubiquitin-conjugating enzymes (E2), and ubiquitin ligases (E3). Addition of ubiquitin to substrate proteins targets them for degradation by the proteasome.

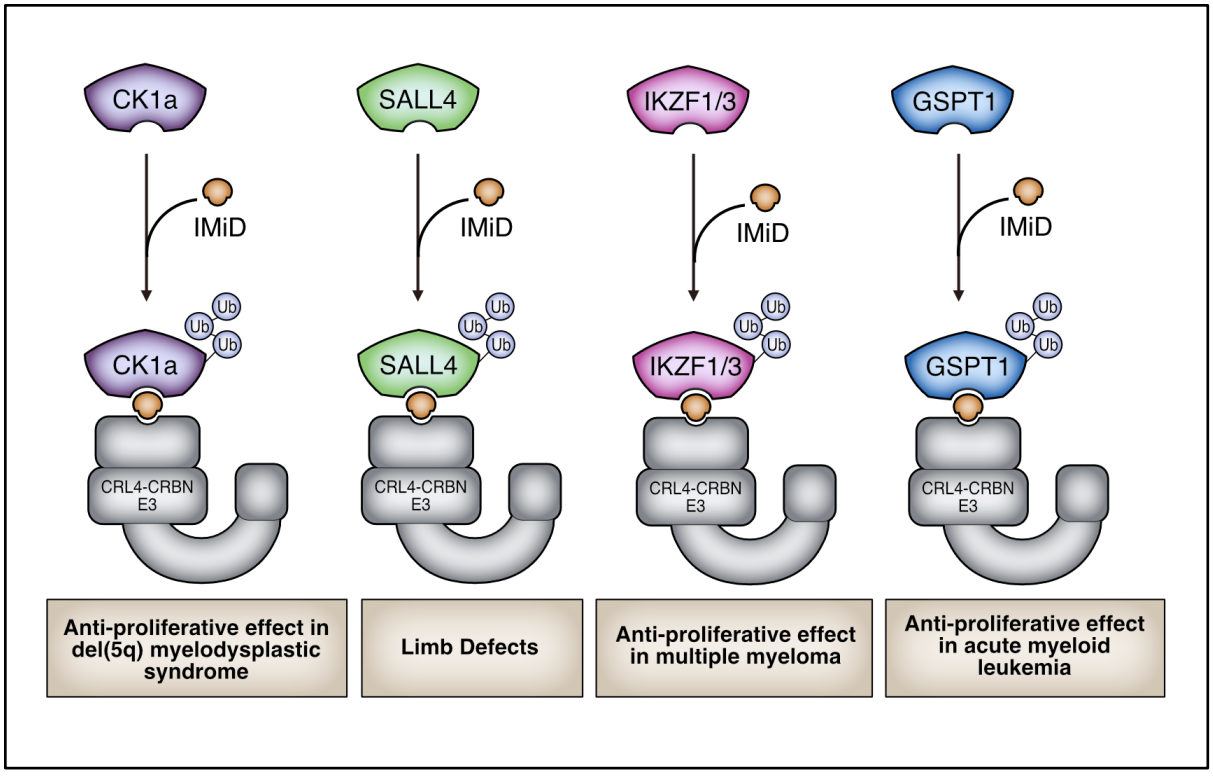

Figure 1-2. Ubiquitination of IMiD substrates.

IMiD compounds target a variety of substrates to the CRL4-CRBN E3 ubiquitin ligase. Substrate ubiquitination and subsequent proteasomal degradation lead to teratogenicity or impaired cancer cell growth.

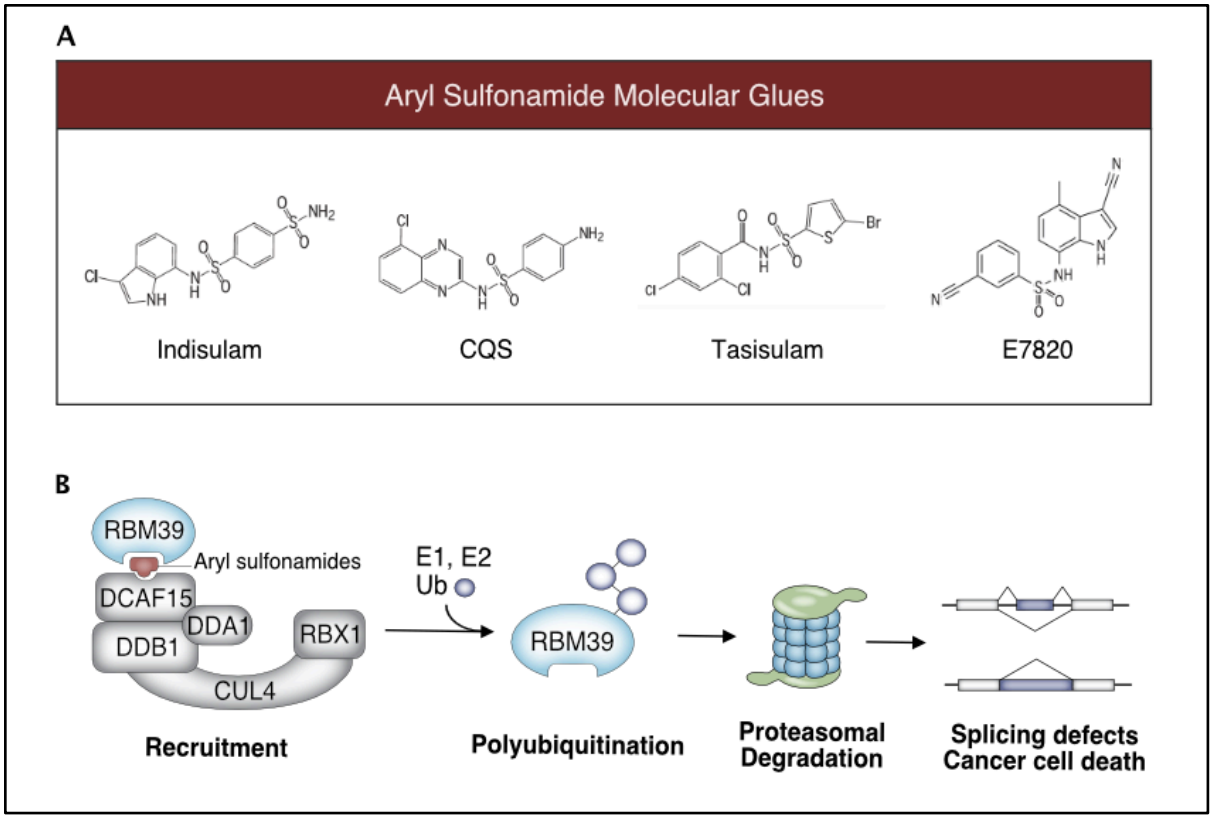

Figure 1-3. Aryl sulfonamide class of molecular glues.

A) Chemical structures of compounds in the aryl sulfonamide class. CQS, chloroquinoxaline sulfonamide. B) Mechanism of action for aryl sulfonamides. Sulfonamides recruit RBM39 to the CRL4-DCAF15 E3 ligase resulting in RBM39 ubiquitination, RBM39 degradation, splicing defects, and cancer cell death.

CHAPTER TWO: IDENTIFICATION OF THE MINIMAL COMPONENTS SUFFICIENT FOR RECONSTITUTING RBM39 UBIQUITINATION *IN VITRO*

Introduction

RBM39 is the only known substrate recruited by the aryl sulfonamide class of molecular glues. Previously, immunoprecipitation and genetic studies demonstrated that RBM39 degradation is dependent on the function of the CRL4-DCAF15 E3 ubiquitin ligase (Han et al., 2017). This E3 ligase complex is composed of a Cullin-4A or Cullin-4B scaffold, RING finger protein Rbx1, substrate receptor DCAF15, adaptor protein DDB1, and a regulatory protein DDA1. Studies conducted in our lab demonstrated that expression of a dominant negative CUL4 mutant, or CRISPR-mediated genetic disruption of DCAF15, DDB1, or DDA1 impaired RBM39 degradation *in vivo.* These results provided evidence that the CRL4-DCAF15 E3 ligase is necessary for RBM39 ubiquitination (Han et al., 2017).

To establish a biochemical system for structural and functional studies of RBM39, we sought to reconstitute RBM39 ubiquitination *in vitro.* Our aim was to develop a model to identify the requirements for RBM39 recruitment and ubiquitination, and then utilize this information to guide discovery of other substrates. Reconstitution presents several advantages. First, distilling a reaction down to isolated, well-characterized components would allow us to distinguish between components that are necessary versus components that are sufficient for ubiquitination. From this system, we would be able to identify domains and modifications required for each protein to function in the complex. Proteins used for

reconstitution reactions could also serve as sources for structural studies including crystallography or cryo-electron microscopy. Finally, a reconstituted system would allow for precise control over the parameters of the ubiquitination reaction, and enable quantification of various aspects of the reaction including binding kinetics.

Purification of CRL4-DCAF15 E3 Ligase and RBM39

To reconstitute RBM39 ubiquitination *in vitro*, we utilized an SF9 insect cell system to express and purify recombinant RBM39 and the CRL4-DCAF15 E3 ligase (Figure 2-1A). These purified E3 ligase components included a complex consisting of the Cul4a scaffold and a truncated version of the RING protein Rbx1 Δ1-14, and a second complex consisting of full-length DCAF15, DDB1, and DDA1 (Figure 2-1A).

In many reconstitution efforts, protein biochemistry is a bottleneck and the purification of the CRL4-DCAF15 E3 ligase was no exception. One of the major challenges in protein purification involved expression of the Cullin-4A scaffold. Insect cell protein expression generally requires the generation of a bacmid encoding the gene of interest, and transfection of this bacmid into insect cells for baculovirus production. The resulting baculovirus is then used to infect cells for protein production. Our previous attempts to obtain bacmid encoding the Cullin-4A gene were unsuccessful. To troubleshoot, we first expressed full-length Cullin-4A along with Rbx1 from the mammalian 293T cell line. We then purified these proteins before placing it into a ubiquitination reaction along with purified RBM39, DCAF15, DDB1, and DDA1. Although the yield of purified Cullin-4A from mammalian cells was modest, we were able to detect evidence of RBM39 ubiquitination by

western blot analysis (data not shown). With a positive result in hand, we then proceeded to optimize Cullin-4A purification in insect cells. We found that we were able to generate bacmid for a truncation mutant of Cullin-4A with a deletion of the first 37 amino acids, but was unable to generate bacmid for full-length Cullin-4A. Therefore, we proceeded to introduce synonymous mutations into the N-terminal region of Cullin-4A. With this change, we were finally able to obtain bacmid containing the full-length Cullin-4A insert and express the protein (Figure 2-1B).

Once all proteins had been purified, we placed them in a ubiquitination reaction mixture containing ubiquitin, E1 enzyme, an ATP source, indisulam, and a panel of commercially available E2 enzymes. Western blotting with an RBM39 antibody revealed the presence of high molecular weight species in the presence of UbcH5a, UbcH5b, or UbcH5c E2 enzymes (Figure 2-2A). To confirm that this species was ubiquitinated RBM39, we performed a dropout experiment in which we sequentially removed one of the components of the reaction. Removal of ubiquitin, indisulam, E1 enzyme, E2 enzyme, Cul4a-Rbx1, or DCAF15-DDB1-DDA1 greatly decreased the levels of this high molecular weight species (Figure 2-2B). In the absence of E1 enzyme, we were still able to detect a low level of RBM39 ubiquitination, which we hypothesized might be due to the presence of a contaminating E1 enzyme that co-purified with one of our recombinant proteins. We then compared RBM39 ubiquitination mediated by different aryl sulfonamides including indisulam, tasisulam, and chloroquinoxaline sulfonamide (CQS). All three sulfonamides were capable of mediating RBM39 ubiquitination to a similar extent (Figure 2-2C).

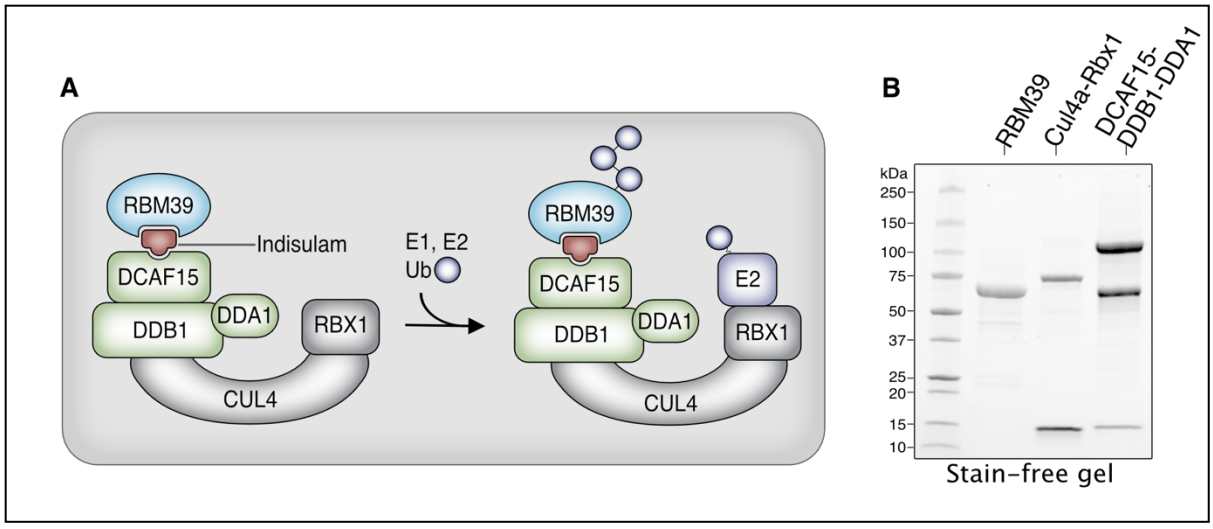

Figure 2-1. Schematic model for *in vitro* reconstitution of RBM39 ubiquitination.

(A) Schematic diagram illustrating a model of indisulam-dependent ubiquitination of RBM39 by the CRL4-DCAF15 E3 Ubiquitin Ligase**.** (B) Stain-free gel of recombinant proteins expressed and purified from SF9 insect cells.

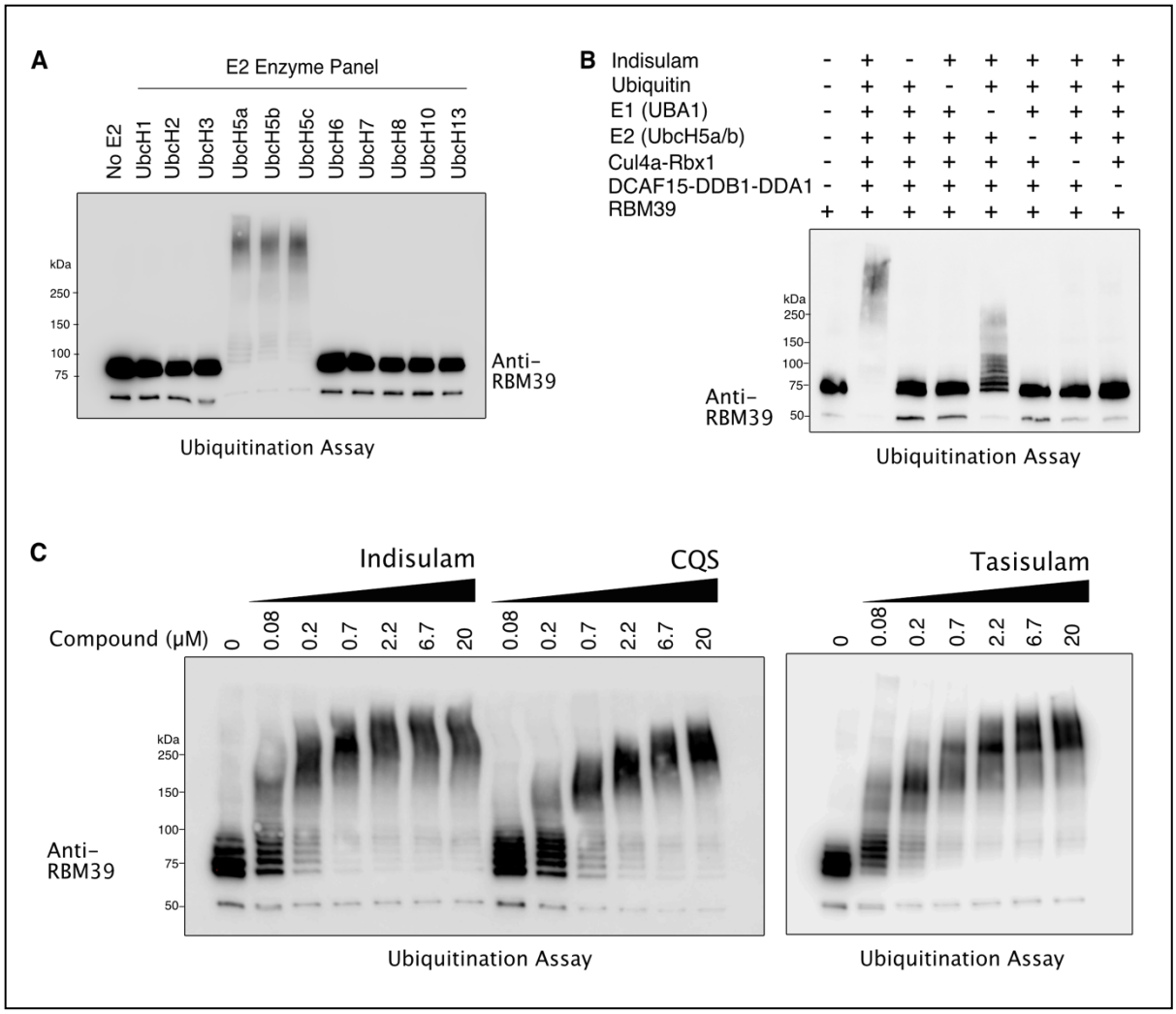

Figure 2-2. Reconstitution of RBM39 ubiquitination *in vitro*.

(A) RBM39 can be ubiquitinated *in vitro* by E2 enzymes UbcH5a, UbcH5b, and UbcH5c. Purified RBM39 was combined with CRL4-DCAF15 E3 ligase complex and screened in a ubiquitination assay against a panel of E2 enzymes (Enzo). Samples were analyzed by western blot with anti-RBM39. (B) Dropout of individual components of the RBM39 ubiquitination mixture was performed to determine the minimal components required for RBM39 ubiquitination, which was analyzed by western blot with anti-RBM39. (C) RBM39

ubiquitination *in vitro* occurs in a dose-dependent manner with the three sulfonamides indisulam, chloroquinoxaline sulfonamide (CQS), and tasisulam.

Discussion

Discovery of sulfonamide-dependent recruitment of RBM39 to the CRL4-DCAF15 E3 ligase represented a major advancement for the field of targeted protein degradation. To elaborate on our understanding of the machinery sufficient for RBM39 ubiquitination, we reconstituted the reaction *in vitro*. Here, we determined that the components sufficient for RBM39 ubiquitination are a sulfonamide, an energy source, ubiquitin, E1 and E2 enzymes, and the CRL4-DCAF15 E3 ligase. Although we did not discover any novel components required for this ubiquitination event, our results are consistent with previous genetic studies of RBM39 in cell culture models.

One goal for developing this system was to discover new substrates by reconstituting ubiquitination activity using a substrate source such as cell lysates, tissue, or protein microarrays. In the past, this technique was used successfully to identify targets of proteins such as the E2/E3 hybrid enzyme UBE2O (Nguyen et al., 2017). In these studies, recombinant ubiquitination enzymes were combined with lysates that were treated with N-ethylmaleimide (NEM) to inhibit endogenous proteins containing cysteine residues. Unfortunately, this technique was not successful for our CRL4-DCAF15 ubiquitination system since only endogenous E1 and E2 enzymes contained catalytic cysteines that could be alkylated and thus inhibited in this manner (data not shown). When we attempted to add purified CRL4-DCAF15 complex with NEM-treated lysates, we detected a high level of background ubiquitination signal. Through dropout experiments, we were able to attribute this signal to the activity of endogenous Cullins, which do not require catalytic cysteines for activity and therefore are not inhibited by NEM-mediated alkylation. Addressing this

problem will require the development of alternative approaches, such as an orthogonal ubiquitin transfer system in which mutant recombinant enzymes only associate with each other and not with their endogenous counterparts (Bhuripanyo et al., 2018; Wang et al., 2017; Zhao et al., 2012).

Another component that would allow this system to more closely mimic physiological conditions is neddylation, a process in which a small ubiquitin-like protein is attached to the Cullin scaffold. This modification is required for Cullin function *in vivo*, and involves a pathway with several neddylation-specific enzymes (Enchev et al., 2015; Huang et al., 2005; Scott et al., 2014; Walden et al., 2003). Reconstitution of both NEDD8 addition (neddylation) and removal (deneddylation) has been performed for Cullin complexes (Cavadini et al., 2016; Duda et al., 2008; Lyapina et al., 2001). Modeling dynamics of neddylation and deneddylation would likely provide insight into the function of components of the CRL4-DCAF15 E3 ligase, particularly for proteins such as DDA1 whose function is still unclear.

In summary, we have reconstituted RBM39 ubiquitination by the CRL4-DCAF15 E3 ligase using components previously shown to be necessary for RBM39 degradation *in vivo.* Further development of this *in vitro* system may eventually lead to its utility as a tool for identifying substrates or studying E3 ligase function.

Experimental Procedures

Recombinant Protein Expression and Purification

The human genes encoding full-length RBM39, full-length DCAF15, full-length DDB1, and Rbx1 lacking the first 14 amino acids (Rbx1Δ1-14) were cloned into pFastBac vectors for the production of N-terminal His-tagged or untagged proteins. For Cul4a expression, attempts to generate baculovirus of full-length Cul4 were unsuccessful until synonymous mutations were introduced into the nucleotide sequence encoding the first 44 amino acids. Cul4a amino acids 2-44 were mutated to the following sequence: GCAGACGAAGCACCACGTAAAGGTAGTTTTTCAGCCTTAGTTGGTCGTACTAATG GTTTAACGAAACCAGCAGCATTAGCAGCAGCACCGGCAAAACCAGGTGGTGCAG GCGGCTCCAAGAAGCTGGTG. Mutated Cul4a was then His-tagged at the N-terminus and cloned into pFastBac for SF9 insect cell expression. Baculoviruses were generated according to vendor's instructions, and used to infect SF9 cells for expression. Cells were harvested 48 hrs after baculovirus infection.

For purification of His-tagged RBM39, cells were resuspended in buffer containing 40 mM Tris, 1M NaCl, 0.1% NP40, 5 mM DTT, 1x SigmaFAST Protease Inhibitors, pH 7.5. The cell suspension was sonicated for 12 cycles at 10s per cycle, with 30s of cooling between cycles at 4°C. Lysate was centrifuged at 35000 rpm for 30 min, and incubated with Ni-NTA agarose for 30 min with rotation at 4°C. Beads were washed three times in wash buffer (40 mM Tris, 1M NaCl, 20 mM imidazole, 5 mM DTT, pH 7.5). Protein was then eluted with elution buffer (40 mM Tris, 1M NaCl, 300 mM imidazole, 5 mM DTT, pH 7.5) and

concentrated to 500 µL. Concentrated protein was injected onto a Superdex200 10/300 column (GE Healthcare). RBM39 protein eluted at 14 ml and was stored at -80°C in 40 mM Tris, 1M NaCl, 1mM TCEP, pH 7.5.

For purification of the DCAF15-DDB1-DDA1 complex, His-tagged DCAF15 was co-expressed with untagged DDB1 and DDA1 in SF9 cells. Cells were resuspended in buffer containing 20 mM Tris, 200 mM NaCl, 0.5% NP40, 1mM TCEP, 1x SigmaFAST protease inhibitors, pH 7.5. Cell suspension was sonicated for 12 cycles at 10s per cycle, with 30s of cooling between cycles at 4°C. Lysate was clarified by centrifugation at 35000 rpm for 30 min, and incubated with Ni-NTA agarose for 30 min at 4°C. Beads were washed three times in wash buffer (20 mM Tris, 200 mM NaCl, 20 mM imidazole, 1mM TCEP, pH 7.5) and eluted with elution buffer (20 mM Tris, 200 mM NaCl, 300 mM imidazole, 1 mM TCEP, pH 7.5). Protein was concentrated and injected onto a Superdex200 Increase 10/300 column (GE Healthcare). The DCAF15-DDB1-DDA1 complex eluted at 13 mL. This peak was collected and further purified by anion exchange chromatography using a HiTrapQ column (GE Healthcare). The protein complex was immediately flash-frozen and stored at 80°C.

For purification of the Cul4a-Rbx1 complex, synonymously mutated His-Cul4a was coexpressed with His-Rbx1Δ1-14 in SF9 cells. Cells were resuspended in buffer containing 50 mM Tris, 200 mM NaCl, 0.1% Triton X-100, 1mM TCEP, and 1x SigmaFAST Protease Inhibitors, pH 8.0. Cell suspension was sonicated for 12 cycles at 10s per cycle, with 30s of cooling between cycles at 4°C. Lysate was centrifuged at 35000 rpm for 30 min, and incubated with Ni-NTA agarose for 30 min with rotation at 4°C. Beads were washed with wash buffer (50 mM Tris, 200 mM NaCl, 10 mM imidazole, 1mM TCEP, pH 8.0) and eluted

with elution buffer (50 mM Tris, 200 mM NaCl, 300 mM imidazole, 1mM TCEP, pH 8.0). Eluate was injected onto a Superdex200 Increase 10/300 column (GE Healthcare), and the protein complex eluted at 13.8 mL. Protein was concentrated and stored at -80°C in 50 mM Tris, 200 mM NaCl, 1mM TCEP, pH 8.0.

In vitro ubiquitination reactions

Recombinant human Cul4a-Rbx1(Δ1-14), DCAF15-DDB1-DDA1, and RBM39 (full-length) were combined with E1 enzyme (UBA1, Boston Biochem), E2 enzyme (UbcH5a and UbcH5b, Boston Biochem), and ubiquitin (Boston Biochem). For E2 enzyme optimizations (Figure 2-2A), individual enzymes from the E2 panel (Enzo) were added to the reaction at concentrations recommended by the vendor. Final concentrations of proteins in the ubiquitination reaction were the following: 0.2 μM UBA1, 0.5 μM UbcH5a, 0.5 μM UbcH5b, 0.8 μM Cul4a-Rbx1, 1 μM DCAF15-DDB1-DDA1, 0.2 μM RBM39, and 100 μM ubiquitin. Proteins were incubated at 30°C for 1.5hr with agitation in a reaction buffer containing 50 mM HEPES (pH 7.5), 5 mM MgCl2, 5 mM ATP, 75 mM sodium citrate, 0.1% Tween20, 1x energy regeneration solution (Boston Biochem) and 0.05% BSA. Reaction mixtures were quenched with loading dye and DTT, followed by SDS-PAGE and immunoblot analysis using RBM39 antibody (Atlas, 1:3000).

CHAPTER THREE: IDENTIFICATION OF REQUIREMENTS FOR RBM39 RECRUITMENT AND UBIQUITINATION

Introduction

Substrates of E3 ubiquitin ligases are recognized by their degrons, which are molecular motifs required for substrate recognition and ubiquitination. Substrates targeted by one class of molecular glue compounds often share a similar degron. For example, the IMiD class of molecular glues targets multiple substrates containing the Cys_2-His_2 (C2H2) zinc finger degron, including IKZF1, IKZF3, and ZFP91. This identification of the IMiD degron led to a screen of a C2H2 zinc finger library, in which 11 additional C2H2 zinc finger-containing substrates were discovered (Sievers et al., 2018). Unlike IMiDs, aryl sulfonamides are currently only known to target one substrate, RBM39. Therefore, we sought to identify the RBM39 degron and to determine whether other aryl-sulfonamide substrates with a similar degron could be discovered. To do this, we determined the sites required for recruitment of RBM39 to the CRL4-DCAF15 E3 ligase, and the lysine residues required for RBM39 ubiquitination.

RBM39 is Ubiquitinated on N-terminal Lysine Residues

Substrate lysine residues often serve as the sites of ubiquitination by E3 ubiquitin ligases. The majority of lysines in RBM39 are located in clusters within the first 135 amino acids at the N terminus (Figure 3-1A). Therefore, we generated RBM39 constructs in which

groups of potential lysine ubiquitination sites were mutated to arginine residues. We then transiently transfected these lysine-to-arginine mutants into 293T cells and evaluated levels with and without indisulam treatment (Figure 3-1B). Each mutant was tagged with an HA epitope tag, which lacks lysines and therefore would not confound interpretation by adding potential ubiquitination sites to the protein. Lysine-to-arginine mutations within the first 60 amino acids of RBM39 did not affect RBM39 degradation (Figure 3-1B). By contrast, mutating the lysines between amino acids 60 and 120 blocked the ability of RBM39 to undergo indisulam-dependent degradation in vivo (Figure 3-1B). This loss of RBM39 degradation was not due to a defect in indisulam-dependent interaction with DCAF15, since all RBM39 lysine-to-arginine mutants we tested were still able to complex with DCAF15 when treated with indisulam (Figure 3-1C). To test whether N-terminal lysines are substrates for ubiquitination *in vitro*, we purified an RBM39 ubiquitination mutant in which all the lysine residues within the first 120 amino acids were mutated to arginine residues (RBM39 K(1-120)R). *In vitro* ubiquitination of the RBM39 K(1-120)R mutant was substantially reduced in comparison to wild-type RBM39 (Figure 3-1D). Both *in vitro* and *in vivo* observations indicate that the primary ubiquitination site of RBM39 is located within the N-terminal 120 amino acids.

The RBM39 RRM2 Domain is Recruited to DCAF15

To identify the minimal binding site of RBM39 required for indisulam-dependent interaction with DCAF15, we generated a panel of RBM39 truncation constructs that lacked either N-terminal or C-terminal sequences (Figures 3-2A). We co-expressed these mutants

with FLAG-tagged DCAF15 in 293T cells and then treated the cells with either DMSO or indisulam. We investigated the ability of each truncated RBM39 protein to co-purify with DCAF15 in comparison to wild-type RBM39. An indisulam-dependent interaction between DCAF15 and RBM39 was not affected by either deletion of the first 249 amino acids of RBM39 (Figure 3-2A) or by deletion of the last 200 amino acids of RBM39 (Figure 3-2B). Any truncation of RBM39 that included an amino acid between 250 and 330 resulted in a decreased interaction with DCAF15. Taken together, we concluded that amino acids 250-330 of RBM39, which corresponds to the RNA-recognition motif 2 (RRM2) domain of RBM39, are necessary to interact with DCAF15. To test whether this domain is sufficient, we compared the interaction of the RBM39 RRM2 to full length RBM39 (Figure 3-2C). The RBM39 RRM2 domain is sufficient for recruitment to DCAF15 in the presence of indisulam.

To quantify the binding affinity of this interaction, we used an *Escherichia coli* system to purify the RBM39 RRM2 domain. We used time-resolved Förster resonance energy transfer (TR-FRET) to measure the impact of indisulam on the binding of RBM39 RRM2 to recombinant DCAF15-DDB1-DDA1. Titration of indisulam to a fixed equimolar ratio of RBM39 RRM2 and DCAF15-DDB1-DDA1 led to a dose-dependent increase in TR-FRET signal (EC_{50} = 2.27 μM) (Figure 3-2D). We have previously demonstrated that the G268V mutation within the RBM39 RRM2 blocks recruitment to DCAF15 (Han et al., 2017). Accordingly, we found that recombinant RRM2 with a G268V mutation does not bind to DCAF15 in the presence of indisulam concentrations as high as 50 μM (Figure 3-2D). These observations collectively demonstrate that the RBM39 RRM2 is the minimal binding domain required for indisulam-dependent recruitment to CRL4-DCAF15.

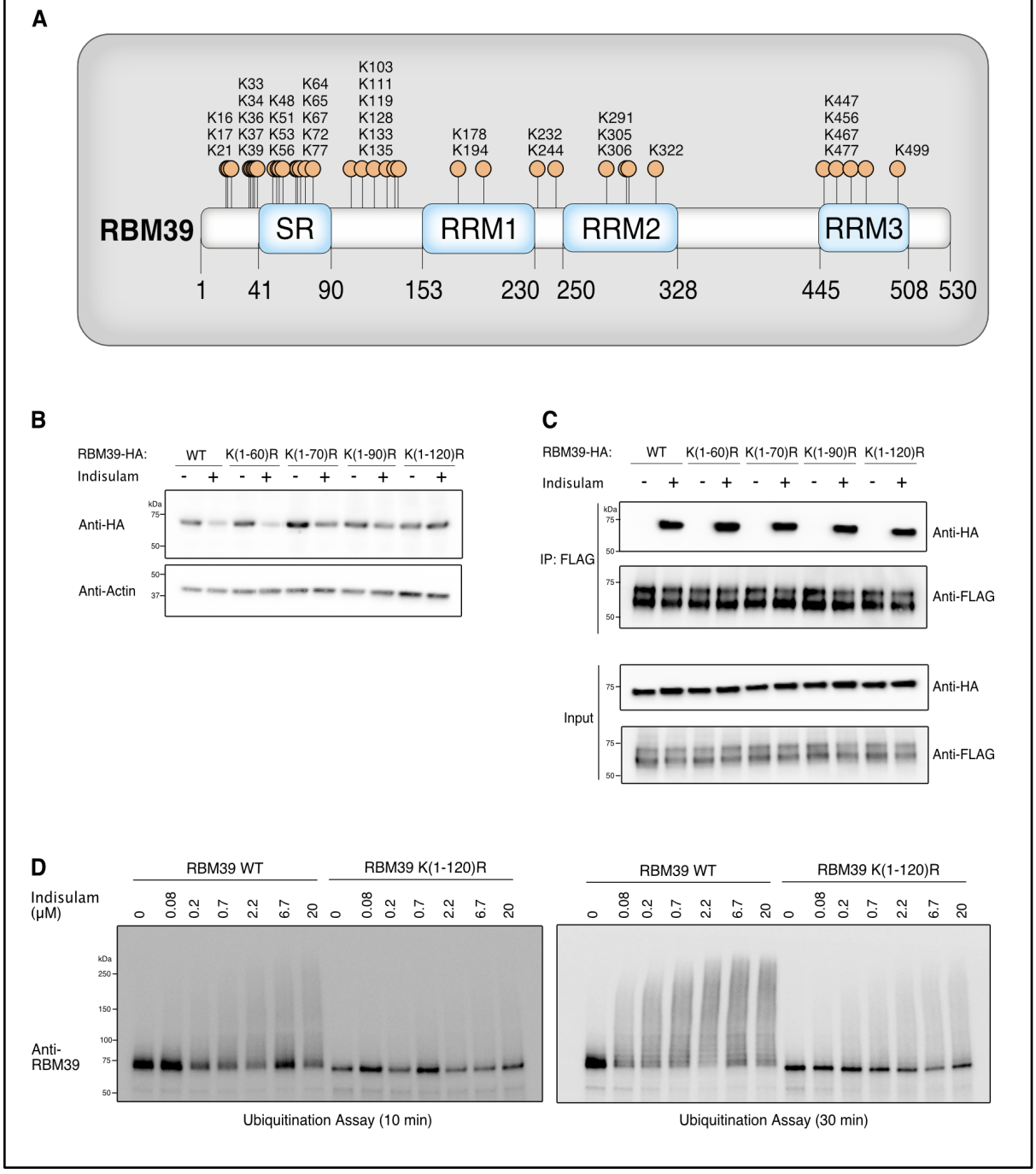
A
K33
K34 K48
K16 K36 K51
K17 K37 K53
K21 K39 K56
K64
K65 K67
K72 K77
K103
K111 K119
K128 K133
K135
K178
K194
K232
K244
K291
K305 K306
K322
K447
K456 K467
K477
K499
RBM39
SR
RRM1
RRM2
RRM3
1 41 90 153 230 250 328 445 508 530
B
RBM39-HA: WT K(1-60)R K(1-70)R K(1-90)R K(1-120)R
Indisulam - + - + - + - + - +
kDa
75
50
Anti-HA
50
37
Anti-Actin
C
RBM39-HA: WT K(1-60)R K(1-70)R K(1-90)R K(1-120)R
Indisulam - + - + - + - + - +
IP: FLAG
Anti-HA
Anti-FLAG
Input
Anti-HA
Anti-FLAG
D
RBM39 WT
RBM39 K(1-120)R
Indisulam (μM)
0 0.08 0.2 0.7 2.2 6.7 20 0 0.08 0.2 0.7 2.2 6.7 20
kDa
250
150
100
75
50
Anti-RBM39
Ubiquitination Assay (10 min)
Ubiquitination Assay (30 min)

Figure 3-1. RBM39 degradation is dependent on N-terminal lysine residues.

(A) Schematic diagram illustrating all potential ubiquitination site lysine residues in RBM39. (B) Mutating lysine residues between amino acids 60–120 of RBM39 blocks indisulam-dependent degradation in vivo. Lysine residues within the indicated RBM39 amino acid regions were mutated to arginine residues. Each mutant was tagged with a lysine-free HA epitope and transfected into 293Ts. Cells were treated with 10 mM indisulam for 6 h, and whole-cell lysates were analyzed by western blotting with anti-HA to assess indisulam-dependent degradation. (C) RBM39 lysine-to-arginine mutants from Figure 3-1B still retain the ability to interact with DCAF15. 293T cells were co-transfected with RBM39-HA and DCAF15-3xFLAG and treated with 1 mM MLN-4924 for 2 h, followed by 10 mM indisulam for 4 h. FLAG immunoprecipitation experiments were performed to examine indisulam-dependent interaction between RBM39 and DCAF15. (D) Mutating lysines within the first 120 amino acids of RBM39 prevents RBM39 ubiquitination *in vitro.* 3xFLAG tagged wild-type RBM39 or the RBM39 K(1-120)R mutant were purified from 293T cells by FLAG immunoprecipitation and subjected to an *in vitro* ubiquitination assay with the indicated concentrations of indisulam. RBM39 ubiquitination was assessed by western blot with anti-RBM39.

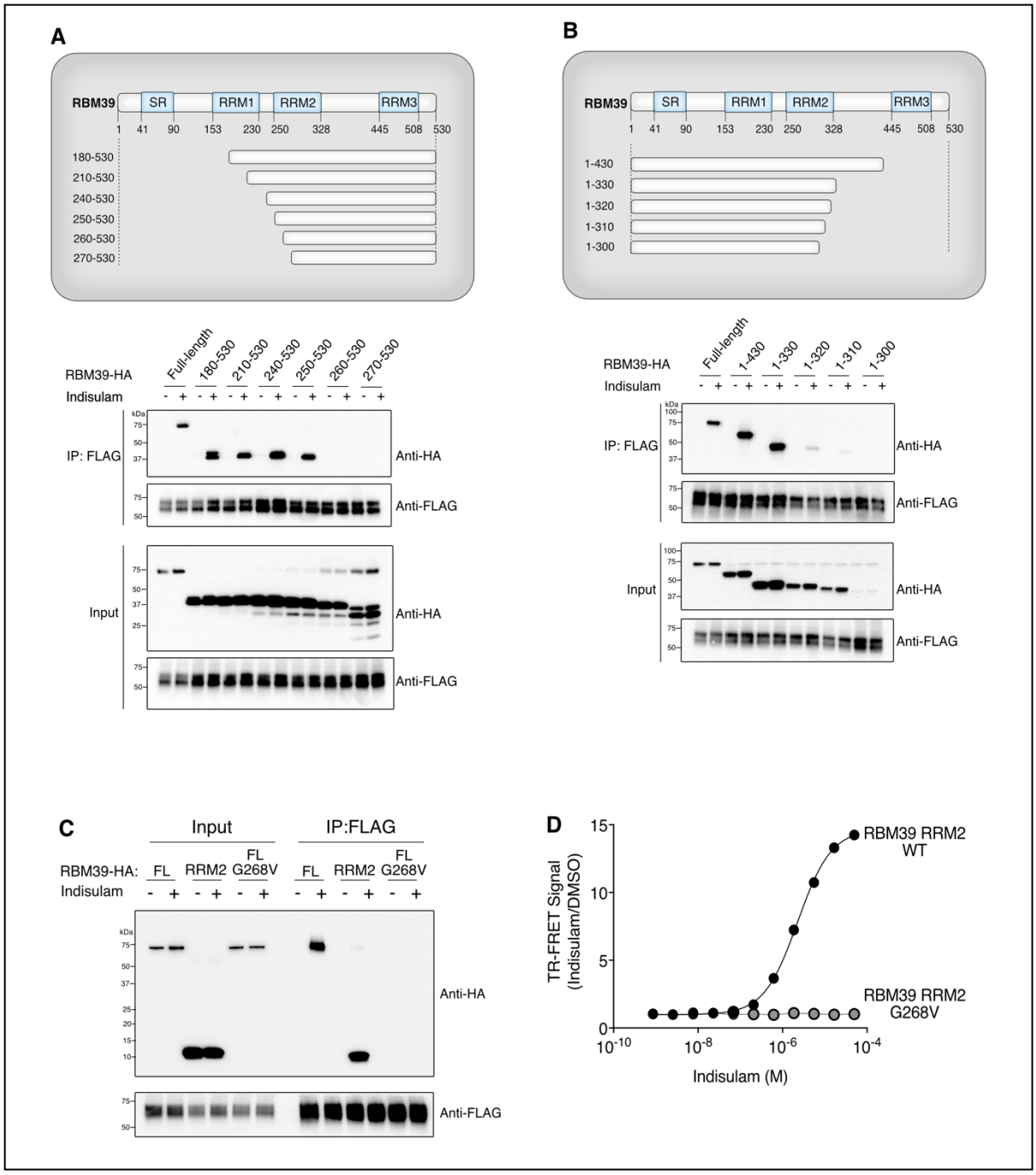
A
RBM39
SR
RRM1
RRM2
RRM3
1 41 90 153 230 250 328 445 508 530
180-530
210-530
240-530
250-530
260-530
270-530
RBM39-HA
Full-length
180-530
210-530
240-530
250-530
260-530
270-530
Indisulam
IP: FLAG
Anti-HA
Anti-FLAG
Input
Anti-HA
Anti-FLAG
B
RBM39
SR
RRM1
RRM2
RRM3
1 41 90 153 230 250 328 445 508 530
1-430
1-330
1-320
1-310
1-300
RBM39-HA
Full-length
1-430
1-330
1-320
1-310
1-300
Indisulam
IP: FLAG
Anti-HA
Anti-FLAG
Input
Anti-HA
Anti-FLAG
C
Input
IP:FLAG
RBM39-HA:
FL
RRM2
FL G268V
Indisulam
Anti-HA
Anti-FLAG
D
TR-FRET Signal (Indisulam/DMSO)
RBM39 RRM2 WT
RBM39 RRM2 G268V
Indisulam (M)

Figure 3-2. RBM39 is recruited to the CRL4-DCAF15 E3 ligase via its RRM2 domain.

(A) The RBM39-binding site for indisulam-dependent interaction with DCAF15 begins at amino acid 250. HA-tagged truncation mutants of RBM39 were co-expressed with DCAF15-3xFLAG in 293T cells. Cells were treated with 1 mM MLN-4924 for 2 h, followed by 10 mM indisulam for 4 h. FLAG immunoprecipitation was performed to identify truncation mutants that still interact with DCAF15. (B) The RBM39-binding site for indisulam-dependent interaction with DCAF15 ends at amino acid 330. FLAG immunoprecipitation experiments were performed with RBM39 truncation mutants, as described in Figure 3-2A. (C) DCAF15 interacts with full-length (FL) wild-type RBM39 and the isolated RBM39 RRM2 domain but not with RBM39 G268V. DCAF15-3xFLAG was co-expressed with RBM39-HA in 293Ts. Cells were treated with 1 mM MLN-4924 for 2 h, followed by 10 mM indisulam for 4 h. FLAG immunoprecipitation and western blots were performed to examine RBM39-indisulam-DCAF15 interactions. (D) Wild-type RBM39 RRM2 but not RBM39 G268V RRM2 binds to DCAF15-DDA1-DDB1 *in vitro*. Time-resolved FRET (TR-FRET) assays were performed by titrating indisulam with RBM39(RRM2)-3xFLAG (amino acids 250–330) purified from *E. coli* and His-DCAF15-DDA1-DDB1 complex purified from SF9 insect cells. The experiment was performed in triplicate, and data are plotted as the mean ± SEM. Some error bars are not visible at the scale of the figure.

Discussion

The majority of current therapeutic molecules target proteins with distinct binding sites like enzymes or receptors. However, many proteins lack binding pockets that are amenable to small molecule design. Molecular glues are an attractive alternative for targeting such proteins, and act by recruiting substrate proteins that contain a specific degron, a critical minimal motif required for ubiquitination by the E3 ligase. Degron identification is usually accomplished by techniques such as alanine scanning, saturation mutagenesis, or deletion mutant analysis (Koren et al., 2018; Sievers et al., 2018; Zhang et al., 2015). Here, we chose the latter approach to identify the RBM39 RRM2 as the domain required for recruitment to the CRL4-DCAF15 E3. This result was consistent with previous data demonstrating that single amino acid mutations within the RBM39 RRM2 block degradation *in vivo* (Han et al., 2017).

Here we also characterized the ubiquitination site of RBM39. Historically, one of the most common methods to identify ubiquitination sites is mass spectrometric analysis (Flick et al., 2004; Peng et al., 2003). In this method, proteins that undergo tryptic digestion will retain a diglycine remnant of ubiquitin. These diglycine-modified peptides can then undergo additional fractionation steps prior to detection by mass spectrometry. We attempted to use this method but failed to obtain adequate coverage of RBM39 by mass spectrometry (data not shown), due to the presence of numerous arginine and lysine residues that served as trypsin cleavage sites. Therefore, we decided to generate lysine-to-arginine mutants in which potential ubiquitination sites were mutated. From this analysis, we found that the major ubiquitination site is located in the N terminal region of RBM39.

Experimental Procedures

Indisulam-dependent degradation assays

For monitoring indisulam-dependent degradation of mutants, RBM39 sequences were cloned into the pcDNA3.1+ vector and tagged with a C-terminal HA tag. 293Ts were seeded in a 6-well plate at 0.5 million cells per well one day prior to transfection. For each well, TransIT:DNA complexes were prepared by combining 200 µL Opti-MEM, 3 µL TransIT-LT1 (Mirus), and 1 µg of DNA (200 ng pcDNA3-RBM23-HA or pcDNA3-RBM39-HA, 400 ng pcDNA3-DCAF15-3xFLAG, 350 ng pcDNA3-3xFLAG, and 50 ng pmaxGFP). Complexes were allowed to incubate at room temperature for 15 min, and then added dropwise to 293T cells. Forty-eight hours after transfection, cells were treated with the indicated doses of indisulam or indoleacetic acid (IAA). Cells were lysed in 1% SDS, with benzonase (Sigma) diluted 1:10,000 in Buffer A (50 mM HEPES 7.4, 10 mM KCl, and 2 mM MgCl2). Samples were analyzed by western blot using HA-HRP antibody (1:3000, 6E2, Cell Signaling Technology) and FLAG-HRP antibody (1:3000, Clone M2, Sigma-Aldrich).

Immunoprecipitation Assays

Anti-FLAG antibody (Clone M2, Sigma-Aldrich) was coupled to Dynabeads M-270 epoxy (Life Technologies) at the concentration of 10 µg of antibody per mg of beads. RBM39 (NM_184234.2) and RBM23 (NM_018107.4) sequences were cloned into the pcDNA3.1+ vector and tagged with a C-terminal HA tag. 293T cells were seeded in 6-well plates at a density of 0.3 million cells per well, and allowed to attach overnight. For each well, transfection complexes were prepared by combining 200 µL Opti-MEM, 3 µL TransIT

LT1 (Mirus), and 1 μg DNA (200 ng pcDNA3-RBM23-HA or pcDNA3-RBM39-HA, 400 ng pcDNA3_DCAF15-3xFLAG, 350 ng pcDNA3-3xFLAG, and 50 ng pmaxGFP). Forty-eight hours after transfection, cells were treated with 1 μM MLN-4924 for 2 hrs followed by 10 μM indisulam for 4 hrs. Cell pellets were collected, washed with PBS, and resuspended in immunoprecipitation (IP) buffer containing 50 mM NaCl, 50 mM NaPO4, 50 mM sodium citrate, 20 mM HEPES pH 7.4, 0.1% Tween, and 1× SigmaFAST protease inhibitor (Sigma-Aldrich). Lysates were centrifuged at 12000 rpm for 10 min at 4°C. Clarified lysates were incubated with 1.5 mg of anti-FLAG magnetic beads for 1 min at 4°C with rotation. Beads were washed three times with IP buffer, followed by elution with 1 mg/ml 3xFLAG peptide (Sigma-Aldrich). Inputs and eluates were analyzed by SDS-PAGE and Western blot analysis using FLAG-HRP (1:3000, Clone M2, Sigma-Aldrich) and HA-HRP (1:3000, Clone 6E2, Cell Signaling Technology) antibodies.

CHAPTER FOUR: ENDOGENOUS SUBSTRATE IDENTIFICATION

Introduction

Despite identification of over 600 E3 ligases, the physiologic substrates for many of these complexes remain unknown. Substrate discovery is notoriously difficult due to several challenges. First, many endogenous substrates may not undergo constitutive degradation and thus may require a stimulus before they can undergo recruitment to an E3 ligase. For example, the E3 ligase c-Cbl binds recognizes substrates after tyrosine phosphorylation (Deckert et al., 1998; Levkowitz et al., 1999; Thien and Langdon, 2001). Another well-known example is hypoxia-inducible factor 1α (HIF1α), a transcription factor that must undergo hydroxylation in the presence of oxygen before it can be ubiquitinated by the von Hippel-Lindau (VHL) E3 ligase complex. During hypoxia, HIF1α is not recognized by the VHL complex and activates genes that encode for pro-angiogenesis proteins, including vascular endothelial growth factor (VEGF) and erythropoietin (Hosoe et al., 1990; Kaelin, 2007; Lerman et al., 1991; Levy et al., 1997; Maxwell et al., 1999; Ohh et al., 2000; Seizinger et al., 1988). Without knowledge of cellular stimuli and post-translational modifications required for substrate recognition, ligase-substrate interactions may be difficult to capture. Another challenge of identifying substrates is due to the redundancy in the ubiquitination system. E3 ligases often have overlapping functions. Substrates may be targeted by different E3 ligases depending on cellular context, both spatially and temporally. Many current methods for substrate identification including immunoprecipitation or *in vitro* reconstitution do not account for regulation by cellular stimuli or cellular

compartmentalization of substrates. Finally, a major obstacle to substrate identification is the transient nature of the intrinsically weak interaction between substrates and ubiquitination machinery. These dynamic interactions are difficult to capture by traditional methods such as immunoprecipitation coupled with mass spectrometry. Some E3-substrate complexes are also characterized by low cellular abundance in addition to rapid dissociation rates, and thus require more sensitive methods for detection. Such challenges necessitate an arsenal of strategies for substrate discovery (Iconomou and Saunders, 2016).

Past strategies found to be effective for substrate identification include global stability profiling to monitor protein stability, *in vitro* ubiquitination using protein microarrays, and proteomics to monitor protein ubiquitination or degradation (Iconomou and Saunders, 2016). Global stability profiling is a fluorescence-based system. This system utilizes a single transcript encoding a putative protein substrate that is tagged with one fluorescent protein (e.g. eGFP), as well as a second fluorescent protein that serves as an internal control. Upon genetic or pharmacological cellular perturbations, protein stability can be monitored by the fluorescence signal ratio between the fluorescently-tagged putative substrate and the internal control. This system has been used to identify SCF substrates, and an adaptation of this system led to the identification of IKZF1 and IKZF3 as neo-substrates for lenalidomide (Lu et al., 2014; Yen and Elledge, 2008; Yen et al., 2008) This approach allows for monitoring of protein dynamics within live cells, but is limited by the labor-intensive difficulty of cloning thousands of proteins into individual constructs and by the presence of potential artifacts arising from overexpression including improper protein localization or folding. In the protein microarray approach, purified ubiquitination machinery is combined with a

library of recombinant proteins (Fischer et al., 2014; Merbl and Kirschner, 2009; Merbl et al., 2013). Ubiquitination events may be detected using radiological, fluorescent, or chemiluminescent readouts to identify proteins that are conjugated to ubiquitin. However, these microarrays do not cover the entire proteome. In addition, recombinant proteins may not accurately reflect their native cellular state and thus may not exhibit proper folding or may lack essential binding partners or PTMs. Finally, the proteomics approach has been one of the most widely used techniques for substrate discovery. Examples of proteomics applications include shotgun proteomics analysis comparing cell lines expressing ubiquitination components against cell lines lacking these components (Iconomou and Saunders, 2016). Affinity purification coupled with mass spectrometry has also been used to enrich for proteins that associate with E3 ligases (Nguyen et al., 2016; O'Connor et al., 2015; O'Connor et al., 2018). In addition, ubiquitinated proteins can be enriched using monoclonal antibodies that recognize the diglycine remnant present on ubiquitinated proteins following tryptic digestion (Kim et al., 2011; Kronke et al., 2014; Udeshi et al., 2013; Xu et al., 2010). Here, we chose to pursue a proteomics approach for substrate discovery because of its relatively unbiased nature and the ability to monitor the levels of proteins *in vivo*.

Currently, RBM39 was the only known substrate of the CRL4-DCAF15 E3 ligase. RBM39 is known as a neo-substrate since it is only recruited to the E3 ligase in the presence of an aryl sulfonamide such as indisulam (Figure 4-1). No endogenous substrates of the CRL4-DCAF15 E3 have yet been discovered to be degraded in the absence of compound. Our goals for identifying endogenous substrates were to discover the physiologic role of the CRL4-DCAF15 E3 ligase, identify the characteristics of substrates ubiquitinated by this E3,

and determine the effects of indisulam on the recruitment and degradation of endogenous substrates.

SILAC-based Mass Spectrometry Approach to Identifying Putative Substrates

Next, we focused on a proteomics approach to monitor changes in protein levels using stable isotope labeling by amino acids in cell culture (SILAC) and mass spectrometry. In contrast to immunoprecipitation, this analysis would provide better insight into the function of the CRL4-DCAF15 E3 ligase rather than relying solely on binding of the DCAF15 substrate receptor to a substrate protein. Immunoprecipitation is also limited by the buffer composition, which may only be able to solubilize a subset of proteins in the proteome and may also affect the kinetics of the interaction between the substrate and E3 ligase. Therefore, we chose this alternative strategy to identify potential substrates.

To identify proteins that might be degraded in a DCAF15-dependent manner, we generated a cell line in which the substrate receptor DCAF15 was deleted, and then re-expressed DCAF15 in the background of this knockout cell line (Figure 4-2). Previously, we had observed that DCAF15 overexpression enhanced RBM39 degradation in the presence of indisulam (Han et al, 2017). Therefore, our hypothesis was that overexpression of the DCAF15 substrate receptor might lead to higher levels of degradation of any endogenous substrates. The DCAF15 knockout line was cultured in light media with unlabeled amino acids, and the DCAF15 re-expression cell line was cultured in heavy media containing $^{13}C_6{}^{15}N_4$-labeled arginine and $^{13}C_6$-labeled lysine (Figure 4-2). After two weeks in culture, cells were lysed and equal amounts of protein from each condition were mixed. The samples

were digested with trypsin and subjected to liquid chromatography-mass spectrometry analysis. We reasoned that deletion of DCAF15 would lead to impaired recruitment of substrates to the CRL4-DCAF15 E3 ligase and thus result in accumulation of any endogenous substrates. Therefore, we compared the abundance of proteins in the DCAF15-expressing line and DCAF15 KO line (Table 4-1). From this list of proteins, we selected fifty of the highest ranking hits for validation studies. Each gene was amplified from cDNA, tagged with a 3xFLAG tag, and cloned into a pcDNA plasmid for expression. The plasmids were transfected in the 293T cell line, and immunoprecipitation assays were then performed to identify proteins that interacted with DCAF15 (data not shown). From this validation assay, proteins that interacted with DCAF15 were further analyzed by *in vitro* reconstitution of ubiquitination. Each target was expressed in 293Ts and then purified under high salt conditions. The purified proteins were then placed in an *in vitro* ubiquitination reaction along with recombinant CRL4-DCAF15 E3 ligase complex. Ubiquitination was monitored with western blot detection of FLAG-tagged protein targets using FLAG antibody (Figure 4-3). In this second assay, two proteins, TMED5 and RPP30, appeared to be partially ubiquitinated *in vitro* as indicated by the formation of higher molecular weight bands with the addition of energy, ubiquitin, and E1/E2/E3 enzymes. This ubiquitination event was dependent on the presence of DCAF15-DDB1-DDA1 and Cul4-Rbx1 as dropout of either of these protein complexes greatly decreased this higher molecular weight signal. We therefore hypothesized that one of these proteins may be a substrate of the CRL4-DCAF15 E3 ligase.

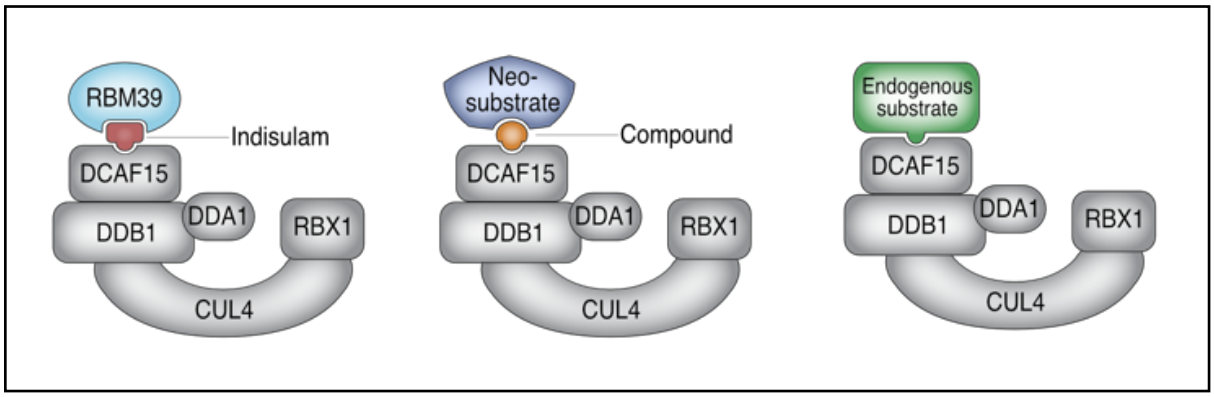

Figure 4-1. Schematic diagram of endogenous and neo-substrates.

Neo-substrates are proteins that are only recruited to the E3 ligase in the presence of a small molecule. RBM39 is an example of a neo-substrate that is recruited to the CRL4-DCAF15 E3 ligase only in the presence of a compound such as indisulam. Endogenous substrates are proteins that are physiologically ubiquitinated by E3 ligases, and may or may not bind to the same pocket as neo-substrates.

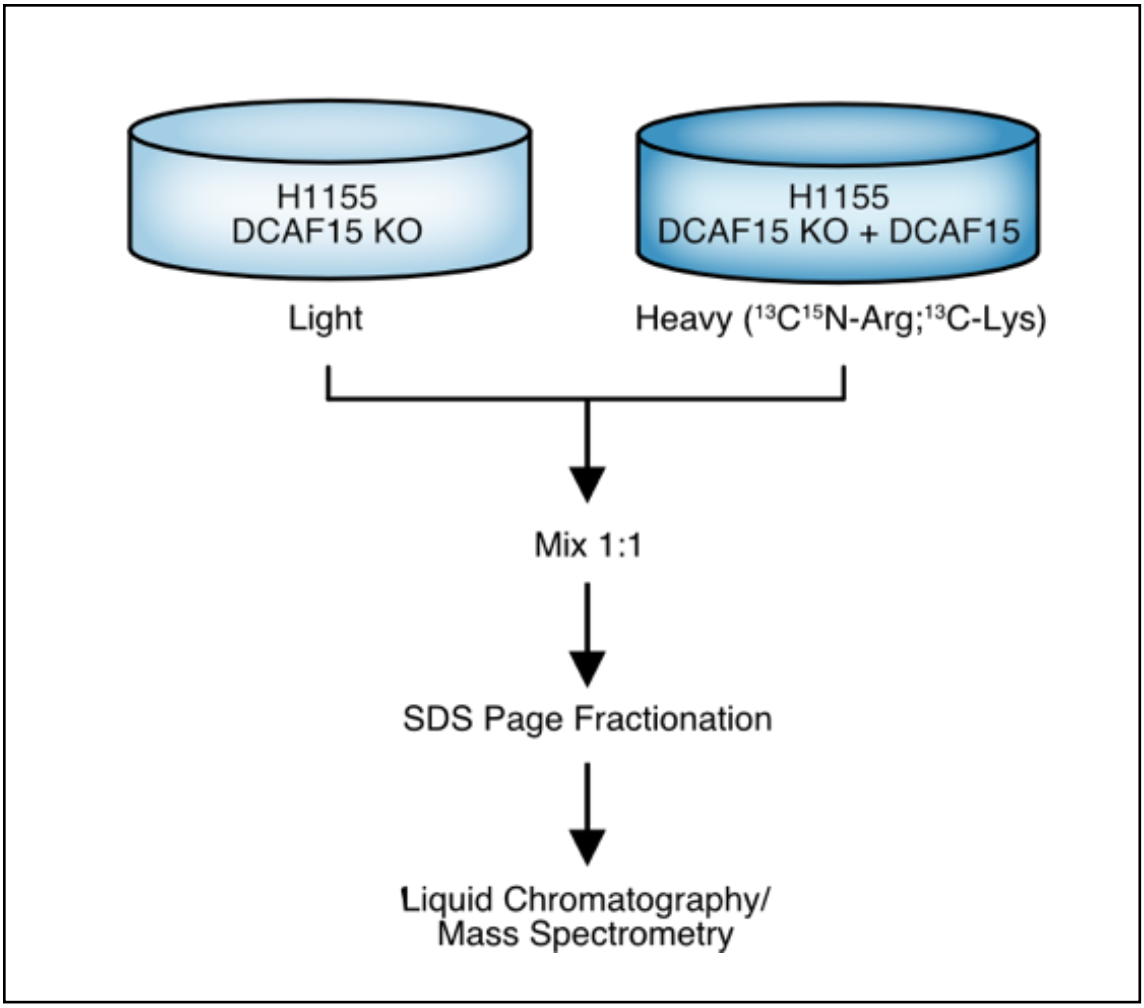

Figure 4-2. Schematic for SILAC-based proteomics discovery of endogenous DCAF15 substrates.

DCAF15 was ablated and then exogenously re-expressed in the H1155 lung cancer cell line. Cell lines were labeled and treated as shown for Stable Isotope Labeling by Amino acids in Cell culture (SILAC)-mass spectrometry analysis.

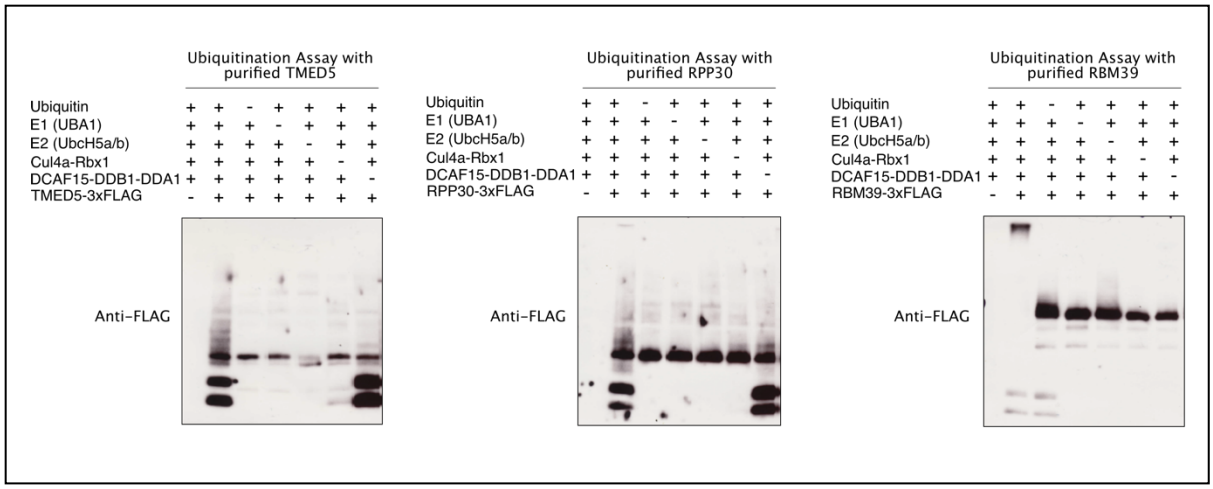

Figure 4-3. *In vitro* ubiquitination validation of putative DCAF15 substrates.

Dropout experiments were performed on FLAG-tagged proteins purified from 293T cells. Ubiquitin, E1, E2, Cul4-Rbx1, or DCAF15-DDB1-DDA1 were sequentially removed from individual reactions. Higher molecular weight signals were monitored by western blotting with anti-FLAG. FLAG-tagged RBM39 was used as a control.

Table 4-1. SILAC-MS proteomics analysis of DCAF15 KO and DCAF15-expressing cells. DCAF15 KO and DCAF15-expressing cells were grown for 2 weeks in light or heavy (^{13}C,^{15}N-Arg; ^{13}C-Lysine) media, respectively. Lysates from both cell lines were combined in equal ratios and submitted for mass spectrometry analysis. Hits were filtered to exclude proteins with <4 peptide counts. Proteins were then sorted by their heavy/light ratios.

Protein	Description	Peptide Count	SILAC Ratio (Heavy/Light)
BTBD17	BTB/POZ domain-containing protein 17	9	0.01
GPATCH8	G patch domain-containing protein 8	7	0.02
HBA1	Hemoglobin subunit alpha	4	0.04
ZNF462	Zinc finger protein 462	6	0.11
MRRF	Ribosome-recycling factor, mitochondrial	5	0.13
FADS1	Fatty acid desaturase 1	4	0.16
MED13	Mediator of RNA polymerase II transcription subunit 13	5	0.17
GALK1	Galactokinase	10	0.22
SPAST	Spastin	4	0.23
NOA1	Nitric oxide-associated protein 1	5	0.23
RNF213	E3 ubiquitin-protein ligase RNF213	25	0.24
FADS2	Fatty acid desaturase 2	10	0.25
DDRGK1	DDRGK domain-containing protein 1	18	0.29
UBE2T	Ubiquitin-conjugating enzyme E2 T	6	0.32
GPRASP2	G-protein coupled receptor-associated sorting protein 2	5	0.32
TAB1	TGF-beta-activated kinase 1 and MAP3K7-binding protein 1	7	0.33
ACOT9	Acyl-coenzyme A thioesterase 9, mitochondrial	11	0.34
DHX57	Putative ATP-dependent RNA helicase DHX57	7	0.35
TRIP13	Pachytene checkpoint protein 2 homolog	4	0.36
ZC3H4	Zinc finger CCCH domain-containing protein 4	7	0.36
PPP1R17	Protein phosphatase 1 regulatory subunit 17	4	0.37
SNX1	Sorting nexin-1	9	0.37
RPP30	Ribonuclease P protein subunit p30	10	0.38
WDR81	WD repeat-containing protein 81	5	0.38
MBLAC2	Metallo-beta-lactamase domain-containing protein 2	4	0.39
BRWD1	Bromodomain and WD repeat-containing protein 1	6	0.39
PODXL2	Podocalyxin-like protein 2	6	0.40

PDCD4	Programmed cell death protein 4	6	0.40
OBSL1	Obscurin-like protein 1	9	0.40
TMED5	Transmembrane emp24 domain-containing protein 5	7	0.41
TRMT1	tRNA (guanine(26)-N(2))-dimethyltransferase	6	0.41
EHBP1	EH domain-binding protein 1	6	0.42
PHIP	PH-interacting protein	15	0.42
ZCCHC11	Terminal uridylyltransferase 4	4	0.42
PDHA1	Pyruvate dehydrogenase E1 component subunit alpha, mito	11	0.44
DACH1	Dachshund homolog 1	4	0.45
TTC27	Tetratricopeptide repeat protein 27	5	0.45
FKBP10	Peptidyl-prolyl cis-trans isomerase FKBP10	8	0.46
BGN	Biglycan	10	0.46
HIP1R	Huntingtin-interacting protein 1-related protein	4	0.46
HMGCS1	Hydroxymethylglutaryl-CoA synthase, cytoplasmic	21	0.46
SMARCA4	Transcription activator BRG1	24	0.46
ERCC2	TFIIH basal transcription factor complex helicase XPD subunit	6	0.46
MARCKS	Myristoylated alanine-rich C-kinase substrate	14	0.46
CYP51A1	Lanosterol 14-alpha demethylase	16	0.47
LSS	Lanosterol synthase	5	0.47
VPS26A	Vacuolar protein sorting-associated protein 26A	11	0.48
PLOD1	Procollagen-lysine,2-oxoglutarate 5-dioxygenase 1	7	0.48
MYCBP2	E3 ubiquitin-protein ligase MYCBP2	26	0.49
OSBPL2	Oxysterol-binding protein-related protein 2	4	0.49
POLA2	DNA polymerase alpha subunit B	5	0.50
FAR1	Fatty acyl-CoA reductase 1	11	0.50
DCAF15	DDB1- and CUL4-associated factor 15	52	26.94

Identification of the Physiologic Role of DCAF15

Little is currently known about the function of the CRL4-DCAF15 E3 ligase. Without knowledge of a phenotype related to DCAF15 function, it is difficult to identify the physiologic conditions under which a substrate is expressed and ubiquitinated by this complex. Substrates may only be expressed in certain tissues under specific cellular stimuli. Therefore, we sought to identify a phenotype dependent on DCAF15 by characterizing a mouse model in which DCAF15 was ablated. To do this, we generated DCAF15 knockout mice using the Easi-CRISPR method (Miura et al., 2018; Quadros et al., 2017). A crRNA targeting exon 1 of the mouse DCAF15 genomic locus along with universal tracrRNA and Cas9 nuclease was used for microinjection (Figure 4-4). Founders were verified by restriction enzyme digestion followed by Sanger sequencing of tail DNA. The DNA sequence surrounding exon 1 of DCAF15 was cloned into plasmids, which were then sequenced by Sanger sequencing to confirm genotypes. Three founders were identified with nucleotide insertions or deletions that resulted in early stop codons (Figure 4-5A). Only Founder 1 was used for subsequent breeding. The DCAF15 mutation associated with Founder 1 resulted in the elimination of an MspA1l site from Exon1 (Figure 4-5B). Therefore, progeny genotypes were verified by restriction enzyme digestion of fragments amplified from tail DNA (Figure 4-5C). Strikingly, we found that we were unable to obtain homozygous DCAF15 mutant mice. The mutant DCAF15 allele could be passed to the offspring only if the female in the breeding pair was heterozygous. We observed that males heterozygous for DCAF15 loss were unable to pass their mutant DCAF allele to offspring

(Figure 4-6). Although a larger sample size is required to confirm these observations, these preliminary results suggest that DCAF15 may be important for spermatogenesis.

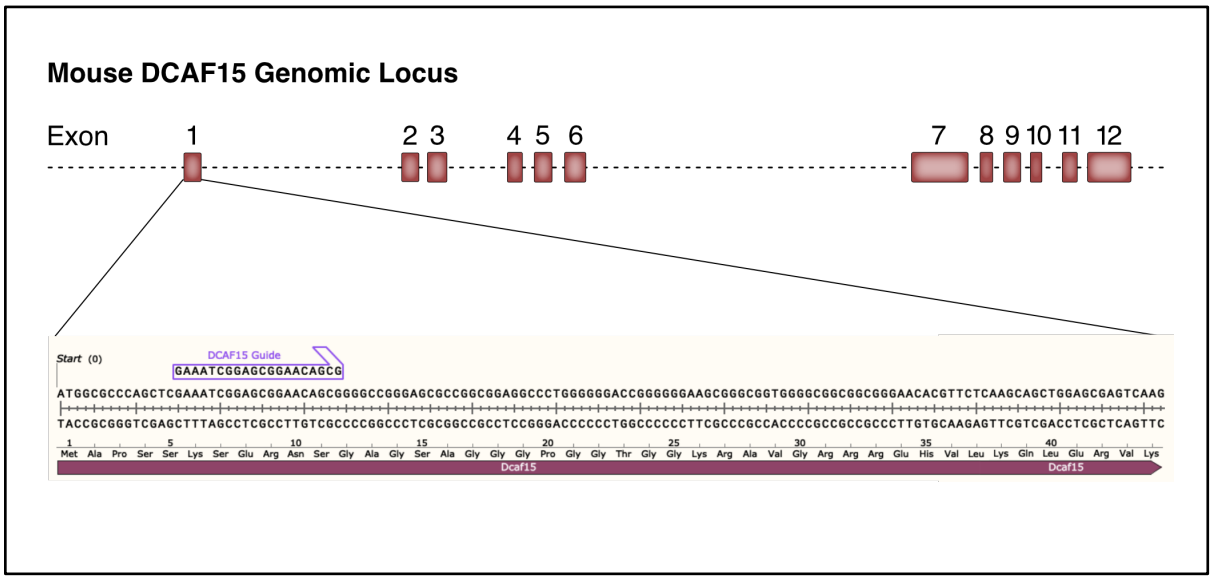

Figure 4-4. Schematic diagram of the mouse DCAF15 genomic locus.

Mutant DCAF15 mice were generated by the Easi-CRISPR method. A single DCAF15 guide was introduced to target Exon 1 of the mouse DCAF15 $_{\text{gene}}$.

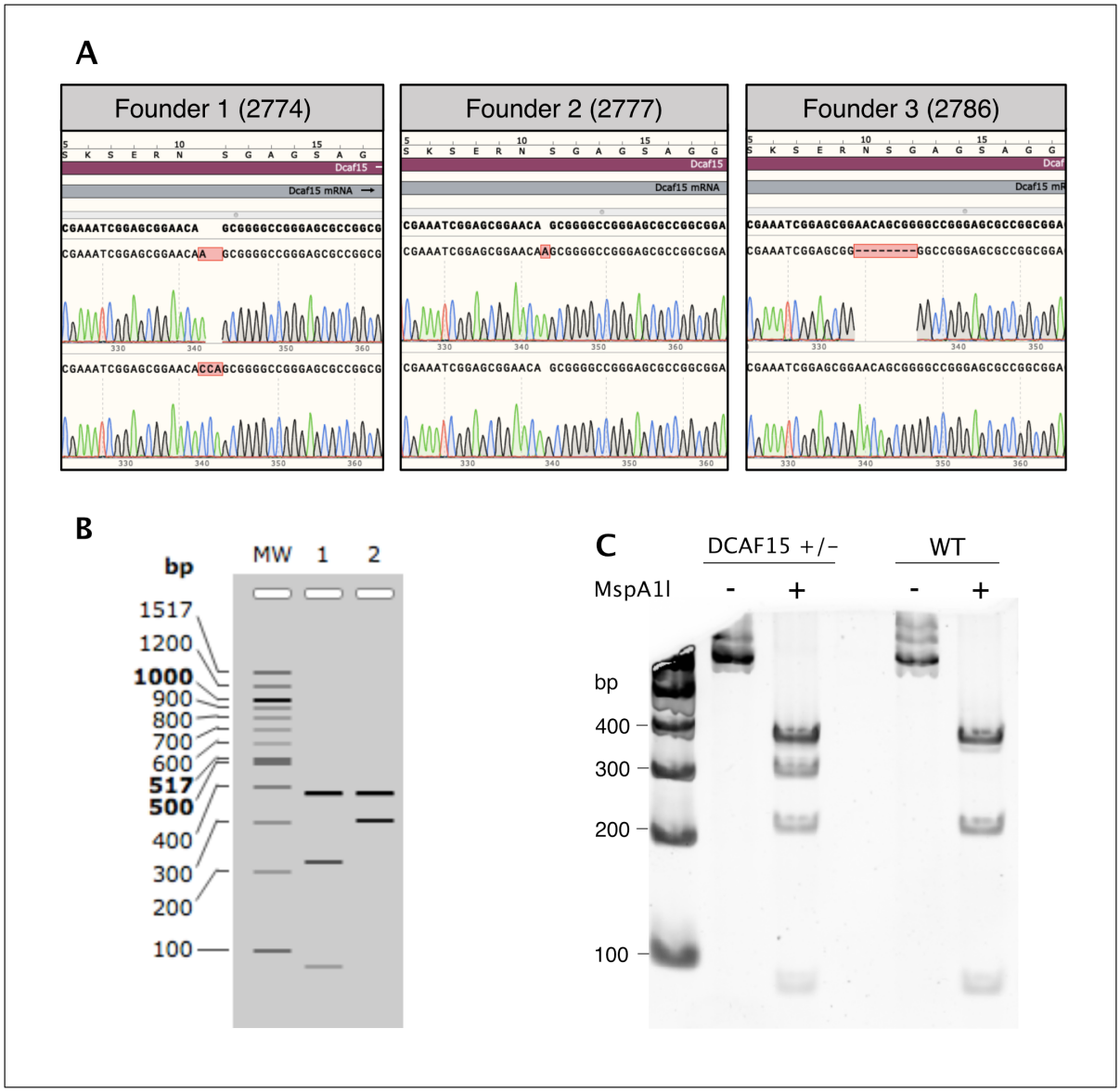

Figure 4-5. Validation of DCAF15 mutant founders.

A) Three female founder mice were identified with DCAF15 mutations. For Founder 1, the first allele contained a single nucleotide insertion, resulting in an early stop codon after amino acid 70. The second allele contained an undesirable 3bp insertion, resulting in the addition of a threonine residue. Breeding schemes for this founder were designed to allow for

propagation of the first allele but not the second. For Founder 2, one allele contained a single nucleotide insertion, resulting in an early stop codon after amino acid 70. For Founder 3, one allele contained an 8bp deletion, resulting in an early stop codon after amino acid 67. B) F1 and F2 generations bred from Founder 1 were genotyped using a restriction digestion method. Founder 1 carried an allele with a 1bp mutation that resulted in the elimination of an MspA1l site. Lane 1 is the banding pattern of genomic DNA from wild-type animals after MspA1l digestion. Lane 2 is the banding of genomic DNA from mutant animals after MspA1l digestion. Heterozygous mice will display both banding patterns. C) Sample gel depicting the restriction digestion patterns of wild-type or heterozygous DCAF15 mutant mice, using the method outlined in (B).

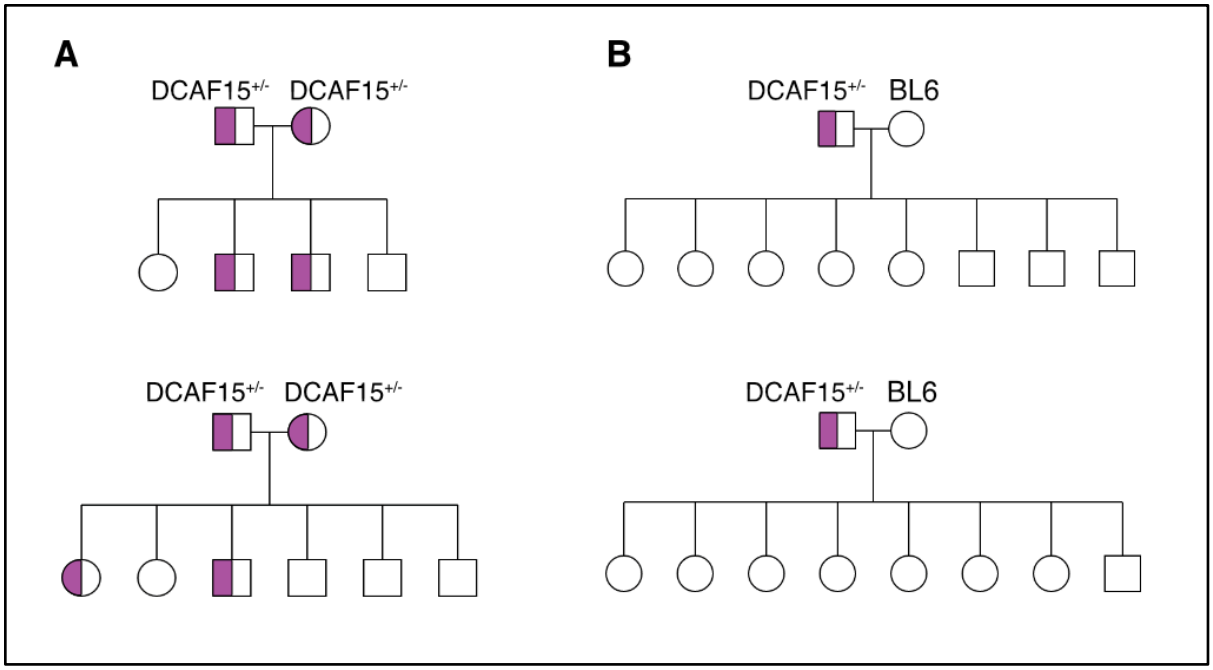

Figure 4-6. Breeding outcomes for DCAF15 mutant mice.

A) Breeding was conducted using the progeny of Founder 1 carrying the mutant DCAF15 allele with a single nucleotide insertion of adenine. Mice were bred with other heterozygous DCAF15 mutant mice carrying the same mutant allele. B) Progeny of heterozygous DCAF15 mutant mice from (A) that were bred with wild-type C57BL/6 mice.

Discussion

Here, we identified two putative substrates of the CRL4-DCAF15 E3 ligase: RPP30 and TMED5. Using an unbiased SILAC-mass spectrometry approach, we determined that the abundance of these proteins is inversely correlated with DCAF15 expression levels. Validation by immunoprecipitation and *in vitro* ubiquitination assays suggested that these two proteins may function as substrates for the CRL4-DCAF15 E3 ligase. Of note, the level of *in vitro* ubiquitination detected for these two putative substrates is much lower than for RBM39 following indisulam addition. This may be due to weaker binding between the substrates and the DCAF15 substrate receptor. Another caveat is that these proteins exist physiologically either in a complex (RPP30) or membrane-bound (TMED5), which may complicate interpretation of these results since our experiments were performed on proteins that are either overexpressed or purified in isolation from other cellular components. Further assays including *in vivo* ubiquitination and degradation assays are required to determine whether these proteins are bona fide substrates for the CRL4-DCAF15 E3 ligase.

Although several proteins from this experiment were shown to interact with DCAF15 by immunoprecipitation, only two of them were shown to undergo ubiquitination *in vitro*. The failure to validate more targets may be due to low expression of endogenous substrates, or due to improper folding, expression, or modification of the proteins that were overexpressed and purified from 293Ts. In addition, some of these proteins may need additional binding partners to adopt the correct conformation for recognition by the E3 ligase. Several caveats to this particular SILAC-MS discovery approach are the presence of secondary effects, such as transcriptional upregulation of DCAF15 substrates in response to

increased degradation by the presence of constitutively overexpressed DCAF15. A better system would involve inducible expression of DCAF15 to physiologic levels for a short period of time in order to reduce effects from cellular compensation. In addition, another caveat is that endogenous DCAF15 substrates may only be expressed under certain stimuli or in certain cell environments such as a specific tissue or cell line, and therefore may not have been detected in this experiment.

In addition to substrate discovery in cell culture models, we also sought to elucidate the endogenous function of the DCAF15 substrate receptor. Here, our goal was to uncover a phenotype that might direct us to a specific tissue or developmental stage in which to discover a CRL4-DCAF15 E3 substrate. To accomplish this, we generated several mice with DCAF15 mutations leading to early stop codons. No defects were observed in female mice. By contrast, male mice with DCAF15 mutations were unable to pass on their allele to progeny, suggesting that DCAF15 may play a role in spermatogenesis. Of interest, several other related members of the Cullin and DCAF families have been associated with spermatogenesis defects in mouse models. Disruption of Cullin-4A has been associated with male infertility due to a defect in meiosis (Hannah and Zhou, 2015; Kopanja et al., 2011; Yin et al., 2011). Disruption of another scaffold with high homology to Cullin-4A, known as Cullin-4B, also leads to male infertility due to defects in post-meiotic sperm development. (Lin et al., 2016; Yin et al., 2016). In addition to Cullin scaffolds, members of the DCAF family also play critical roles in spermatogenesis. For example, deletion of DCAF17 in mice leads to defects in sperm development, resulting in a low number of sperm with abnormal morphology and decreased motility. Mutations in the human DCAF17 gene lead to

Woodhouse-Sakati syndrome, which has been associated with hypogonadism and sperm defects including azoospermia (Agopiantz et al., 2014; Alazami et al., 2008; Ali et al., 2018; Woodhouse and Sakati, 1983).

Interestingly, our observations of DCAF15 indicate that DCAF15$^{+/-}$ mice still remain fertile and only lack the ability to pass their mutant allele to their progeny. This unique phenotype may indicate that DCAF15 plays a distinct role in spermatogenesis. The implication of multiple Cullins and DCAFs in spermatogenesis suggests that these components orchestrate a program of ubiquitination-mediated substrate turnover to regulate sperm development. Further studies are required to identify substrate targets required for normal spermatogenesis, and to delineate the roles of specific E3 ligase components in this process.

Experimental Procedures

SILAC-Mass Spectrometry Analysis

The SILAC base media was prepared by combining RPMI with 5% dialyzed FBS and 1% L-glutamine. Heavy media consisted of SILAC base media supplemented with L-proline, $^{13}C_6{}^{15}N_4$-L-arginine (Arg10), and $^{13}C_6{}^{15}N_2$-L-Lysine (Lys8). Light media consisted of SILAC base media supplemented with L-proline, L-arginine (Arg0), and L-lysine (Lys0). DCAF15 KO cells were grown in light media, and DCAF15 KO cells with lentiviral-mediated expression of DCAF15 were grown in heavy media. Both cell lines were grown for two weeks in labeling media in a humidified atmosphere with 5% CO_2 in air. Cells were then collected, washed with PBS, and solubilized in Buffer A (50 mM HEPES 7.4, 10 mM KCl, 2 mM $MgCl_2$ and 1% SDS). Protein concentration from both samples was quantified using a BCA assay kit (Thermo Fischer). Equivalent amounts of protein from each cell line were combined and fractionated by SDS-PAGE electrophoresis. Gel lanes were excised into 11 pieces and submitted for in-gel digestion and mass spectrometry analysis.

Generation of DCAF15 mutant founders

For the initial validation of founders, genomic DNA was purified from mouse tails using the KAPA mouse genotyping kit. Genomic DNA was then amplified using the following primers: oTT1146 (GACCTGAATATCTTGTCTTCTGAGC) and oTT1148 (GTTTATGGTTTTGATATGCAGACAG). For the final validation of founders, genomic DNA was amplified using primers oTT1281

(TCTACTAGAGGATCTATTTCCGGTGAATTCCTGTTACCATCTTTACCAACCAAAA) and oTT1282 (CGTAATCTGGAACATCGTATGGGTAGGATCATTCCTCGGACAGCTTCTACAGTAA). PCR products were cloned into the pcDNA3.1+ plasmid and sequenced by Sanger sequencing.

Genotyping of DCAF15 mutant mice

Founder 1 (2774) progeny were expected to either carry the wild-type DCAF15 allele or a mutant DCAF15 allele with a single nucleotide insertion of adenine. Since this adenine insertion eliminates an MspA1I restriction site, wild-type and mutant alleles can be distinguished by restriction enzyme digestion. To do this, we isolated mouse tail DNA using the KAPA mouse genotyping kit. We then amplified a portion of the genomic DCAF15 locus using primers oTT1142 (CTGTTACCATCTTTACCAACCAAAA) and oTT1144 (ATTCCTCGGACAGCTTCTACAGTAA). PCR products were purified using the Clontech nucleospin kit and digested with MspA1l. The digestion products run on an ethidium-bromide stained agarose gel (2.5%) and visualized under UV transillumination.

CHAPTER FIVE: NEO-SUBSTRATE IDENTIFICATION

Introduction

Substrate receptors including DCAFs often recruit substrates with similar sequences or structural features, known as degrons (Guharoy et al., 2016; Sievers et al., 2018). Successful identification of degron sequences such as the C2H2 zinc finger motif present in IMiD substrates have led to targeted screens that identified novel neo-substrates. As discussed in Chapter Four, the only known DCAF15 substrate is RBM39. RBM39 requires N-terminal lysines and an RRM2-containing degron for recruitment and ubiquitination by the CRL4-DCAF15 E3 ligase. A closely related paralog of RBM39 is another RNA binding protein known as RBM23 (Dowhan et al., 2005). In a comparison of primary sequences, the RBM23 RRM2 domain has an 88% identity to the RBM39 RRM2, which is sufficient for recruitment to DCAF15 (Figure 5-1). Therefore, we hypothesized that RBM23 may also be recruited to CRL4-DCAF15 by aryl sulfonamides, ubiquitinated, and degraded *in vivo*.

RBM23 Undergoes Indisulam-Dependent Degradation

To test whether RBM23 is a substrate targeted by aryl sulfonamides, we endogenously tagged RBM23 with a C-terminal 3xFLAG sequence in order to monitor RBM23 protein levels (Figure 5-2). Treatment with three different sulfonamides led to a dose-dependent decrease in RBM23-3xFLAG protein (Figure 5-3A). In addition to the predominant FLAG antibody-reactive band, we observed a lower molecular weight band that migrated at 27 kD and decreased with indisulam treatment (Figure 5-3A). This proteoform

may be a cleavage product or alternatively spliced product of RBM23 that still retains its ability to undergo indisulam-dependent degradation. To determine whether degradation of RBM23, like RBM39, is also dependent on DCAF15, we ablated DCAF15 from the endogenously tagged RBM23-3xFLAG line using CRISPR-Cas9 editing. RBM23 degradation was significantly impaired in these cells demonstrating that degradation of RBM23, like RBM39, is DCAF15-dependent (Figure 5-3B). We then tested whether RBM23 degradation was independent of RBM39 degradation. Using CRISPR/Cas9, we engineered an epitope tag into the C-terminus of RBM23 in a previously identified HCT-116 clone that expresses RBM39 with a G268V mutation (Han et al., 2017). Consistent with our previous findings, RBM39 G268V is not degraded by indisulam (Figure 5-3C). By contrast, RBM23 degradation still occurred in an indisulam-dependent manner, demonstrating that RBM23 degradation is independent of RBM39 levels (Figure 5-3C).

Based on these findings, we predicted that the region of RBM23 that interacts with DCAF15 also maps to a region containing the RRM2 domain of RBM23 (Figure 5-4A). To test this hypothesis, we generated a panel of HA-tagged RBM23 truncation mutants and analyzed their ability to co-immunoprecipitate with DCAF15 (Figure 5-4A). We found that the RBM23 binding site mapped to amino acids 210-330, which encompasses the RBM23 RRM2 domain (Figures 5-4B). This RBM23 binding site co-immunoprecipitated with DCAF15 when expressed in 293T cells (Figure 5-4C). We then expressed and purified the RBM23 minimal binding site from *E. coli* and tested its ability to interact with DCAF15-DDB1-DDA1 complex by TR-FRET (Figure 5-4D). Titration of indisulam to a fixed equimolar amount of RBM23 (210-330) domain and DCAF15-DDB1-DDA1 resulted in an

EC50 of 2.58 μM (Figure 5-4E). Introduction of either the RBM39 G268V mutation, or the equivalent G265V mutation in RBM23 prevented indisulam-dependent interaction with DCAF15-DDB1-DDA1 by TR-FRET (Figure 5-4E). Together, these results demonstrate that, similar to RBM39, RBM23 is a neo-substrate that can be recruited to DCAF15 and undergo sulfonamide-dependent degradation.

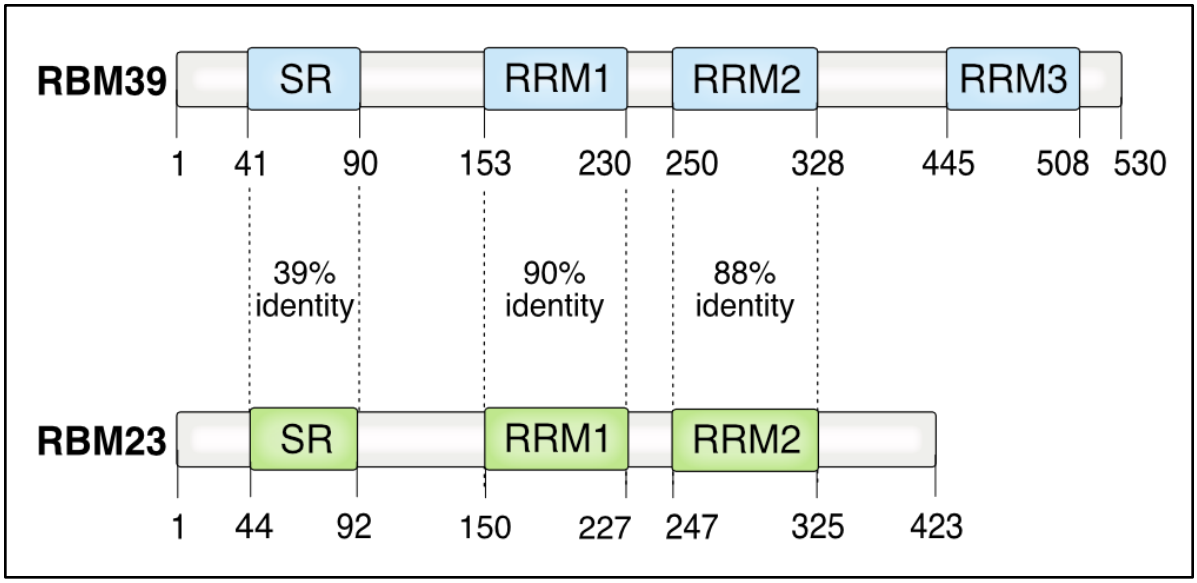

Figure 5-1. Schematic alignment of full-length human RBM23 and RBM39 sequences.

The percentage identity between the serine-arginine rich (SR) domains and RNA recognition motifs (RRMs) are indicated.

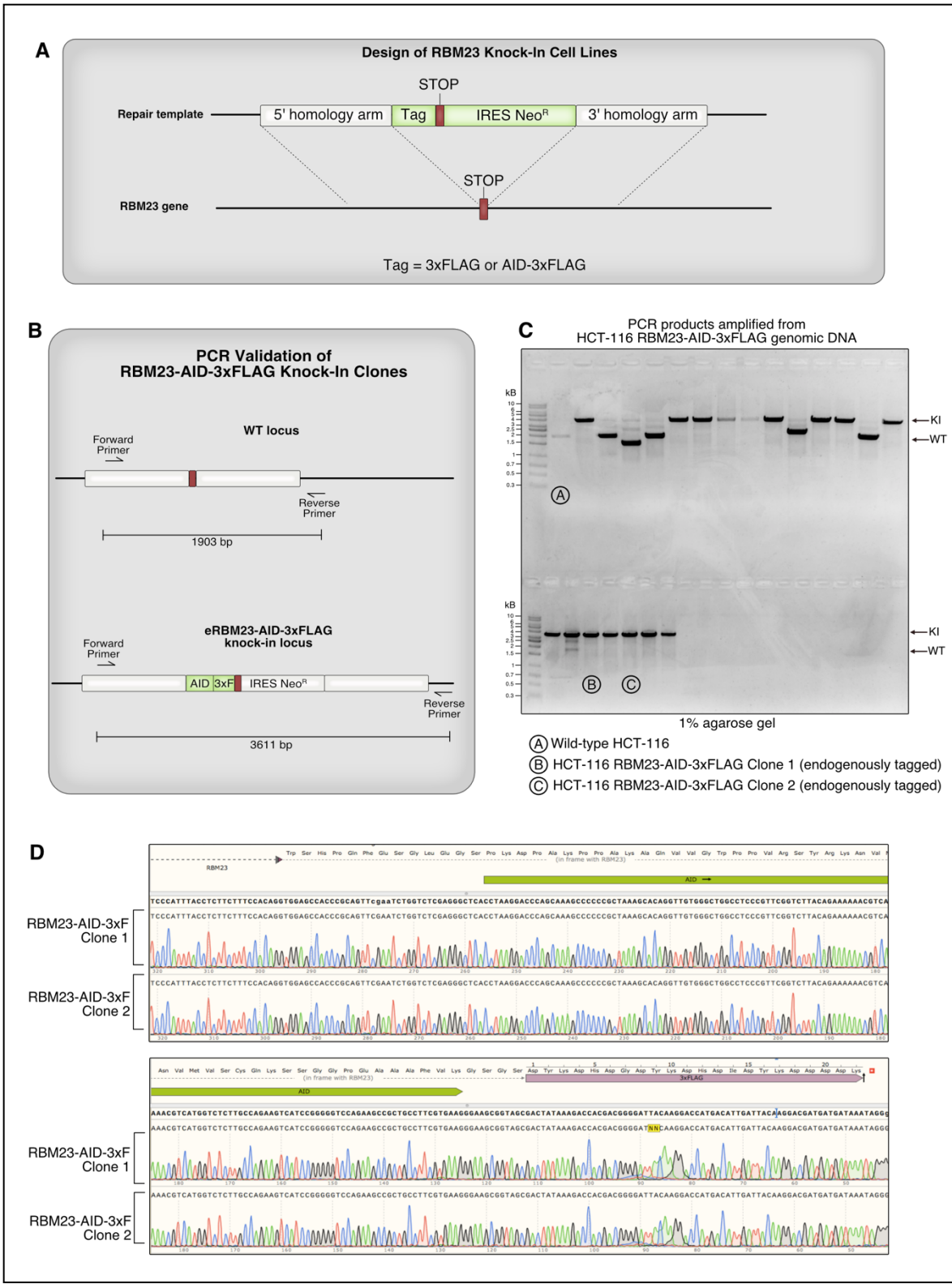
A
Design of RBM23 Knock-In Cell Lines
STOP
Repair template
5' homology arm
Tag
IRES Neo^R
3' homology arm
STOP
RBM23 gene
Tag = 3xFLAG or AID-3xFLAG
B
PCR Validation of
RBM23-AID-3xFLAG Knock-In Clones
WT locus
Forward Primer
Reverse Primer
1903 bp
eRBM23-AID-3xFLAG
knock-in locus
Forward Primer
AID
3xF
IRES Neo^R
Reverse Primer
3611 bp
C
PCR products amplified from
HCT-116 RBM23-AID-3xFLAG genomic DNA
kB
KI
WT
A
B
C
1% agarose gel
A Wild-type HCT-116
B HCT-116 RBM23-AID-3xFLAG Clone 1 (endogenously tagged)
C HCT-116 RBM23-AID-3xFLAG Clone 2 (endogenously tagged)
D
RBM23-AID-3xF Clone 1
RBM23-AID-3xF Clone 2
RBM23-AID-3xF Clone 1
RBM23-AID-3xF Clone 2

Figure 5-2. Generation of endogenously tagged RBM23 cell lines.

(A) Schematic diagram illustrating CRISPR/Cas9 strategy for knocking in tags to the endogenous RBM23 locus. (B) Strategy for validation of tag incorporation in RBM23-AID-3xFLAG endogenously-tagged lines. PCR primers were chosen so that one primer annealed to a genomic region outside of the homology arm. PCR products from wild-type and the RBM23-3xFLAG knock-in cell lines were predicted to be ~1.9 kB and ~3.6 kB, respectively. (C) Homozygous tagging of RBM23 with AID-3xFLAG was confirmed by agarose gel validation of PCR products amplified from the genomic DNA. Clones 1 and 2 are homozygous for knock-in editing. (D) Sequencing results from PCR products amplified from the genomic DNA of RBM23-AID-3xFLAG clones, as analyzed by Sanger sequencing.

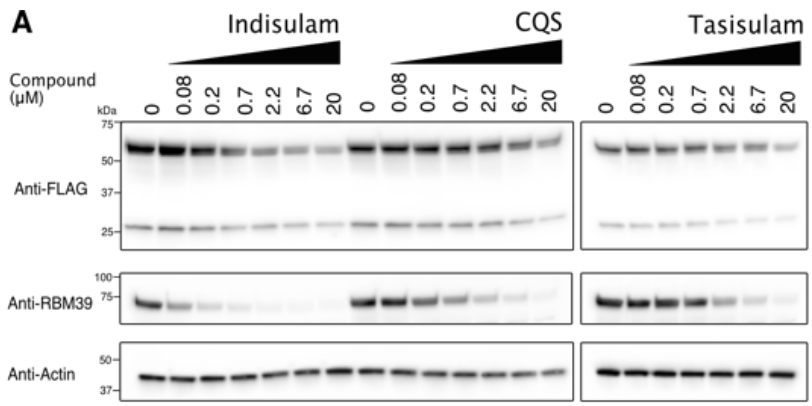
A
Indisulam
CQS
Tasisulam
Compound (μM)
0 0.08 0.2 0.7 2.2 6.7 20
kDa
Anti-FLAG
Anti-RBM39
Anti-Actin

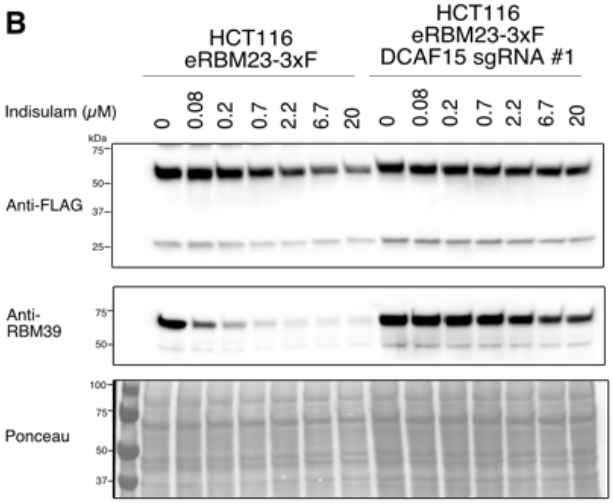
B
HCT116 eRBM23-3xF
HCT116 eRBM23-3xF DCAF15 sgRNA #1
Indisulam (μM)
0 0.08 0.2 0.7 2.2 6.7 20
kDa
Anti-FLAG
Anti-RBM39
Ponceau

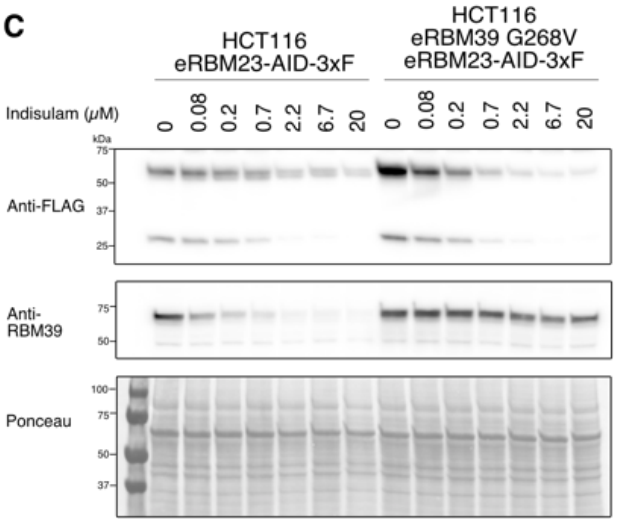
C
HCT116 eRBM23-AID-3xF
HCT116 eRBM39 G268V eRBM23-AID-3xF
Indisulam (μM)
0 0.08 0.2 0.7 2.2 6.7 20
kDa
Anti-FLAG
Anti-RBM39
Ponceau

Figure 5-3. RBM23 is an aryl sulfonamide neo-substrate of the CRL-DCAF15 E3 ligase.

(A) Endogenous RBM23 degrades in a dose-dependent manner with indisulam, CQS, and tasisulam treatment. CRISPR/Cas9 was used to tag the C terminus of RBM23 with 3xFLAG in the HCT-116 cell line. Cells were treated with the indicated compound doses for 24 h and analyzed by western blot using FLAG horseradish peroxidase (HRP) antibody. (B) DCAF15 is required for RBM23 degradation with indisulam treatment. A CRISPR guide against DCAF15 was expressed in an endogenously tagged HCT-116 RBM23-3xFLAG cell line. Cells were treated with the indicated doses of indisulam for 24 h. RBM23 levels were analyzed by western blot using FLAG-HRP antibody. (C) RBM23 degradation is not dependent on RBM39 recruitment to the CRL4-DCAF15. RBM23 was tagged in cell lines with wild-type RBM39 or RBM39 G268V. Cells were treated with the indicated doses of indisulam for 24 h, and RBM23 protein levels were analyzed by western blot using FLAG-HRP antibody.

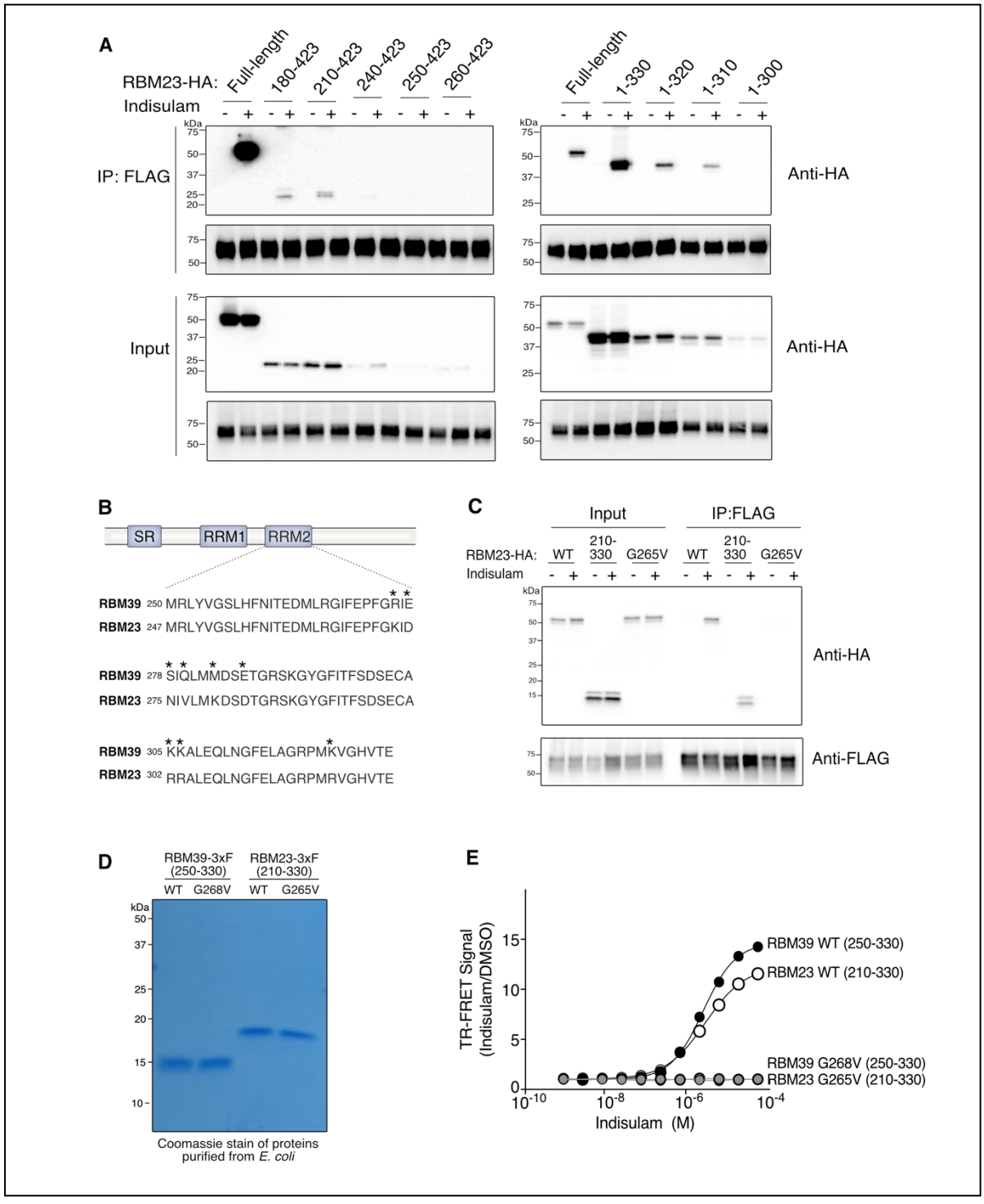
A
RBM23-HA:
Full-length
180-423
210-423
240-423
250-423
260-423
Indisulam
- + - + - + - + - + - +
kDa
IP: FLAG
Anti-HA
Input
Anti-HA
Full-length
1-330
1-320
1-310
1-300
B
SR
RRM1
RRM2
RBM39 250 MRLYVGSLHFNITEDMLRGIFEPFGRIE
RBM23 247 MRLYVGSLHFNITEDMLRGIFEPFGKID
RBM39 278 SIQLMMDSETGRSKGYGFITFSDSECA
RBM23 275 NIVLMKDSDTGRSKGYGFITFSDSECA
RBM39 305 KKALEQLNGFELAGRPMKVGHVTE
RBM23 302 RRALEQLNGFELAGRPMRVGHVTE
C
Input
IP:FLAG
RBM23-HA:
WT
210-330
G265V
Indisulam
Anti-HA
Anti-FLAG
D
RBM39-3xF (250-330)
RBM23-3xF (210-330)
WT G268V WT G265V
kDa
Coomassie stain of proteins purified from E. coli
E
TR-FRET Signal (Indisulam/DMSO)
RBM39 WT (250-330)
RBM23 WT (210-330)
RBM39 G268V (250-330)
RBM23 G265V (210-330)
Indisulam (M)

Figure 5-4. RBM23 is recruited to the CRL4-DCAF15 E3 ligase through an RRM2-containing domain.

(A) The RBM23 binding site for indisulam-dependent interaction with DCAF15 is within amino acids 210-330. HA-tagged truncation mutants of RBM39 were co-expressed with DCAF15- 3xFLAG in 293T cells. Cells were treated with 1 μM MLN-4924 for 2 hrs, followed by 10 μM indisulam for 4 hrs. FLAG immunoprecipitation was performed to identify truncation mutants that still interact with DCAF15. (B) Schematic Diagram with Alignment of the RRM2 domains of RBM39 and RBM23. Differences in the amino acid sequences of RBM39 and RBM23 are indicated by asterisks. (C) DCAF15 interacts with full-length (FL) wild-type RBM23 and the isolated RBM23 amino acid 210-330 region, but not with RBM23 G265V. DCAF15-3xFLAG was co-expressed with HA-tagged RBM23 constructs in 293Ts. Cells were treated with 1 μM MLN-4924 for 2 hrs, followed by 10 μM indisulam for 4 hrs. FLAG immunoprecipitation and western blots were performed to examine RBM23-indisulam-DCAF15 interactions. (D) Purification of RBM39 and RBM23 Binding Sites Required for Indisulam-Dependent DCAF15 Interaction. Recombinant proteins were tagged with 3xFLAG and expressed in Escherichia coli. Proteins were assessed by Coomassie staining. (E) Amino acids 210–330 of RBM23 encompassing the RRM2 interact with DCAF15-DDB1-DDA1 i*n vitro*. TR-FRET assays were performed by titrating indisulam to purified RBM23-3xFLAG (amino acids 210–330) and His-DCAF15-DDA1-DDB1 complex. The experiment was performed in triplicate, and data are plotted as the mean ± SEM. Some error bars are not visible at the scale of the figure.

Discussion

Molecular glues usually target neo-substrates with similar degron sequences. Here we identified a second indisulam-dependent neo-substrate known as RBM23. RBM23 is an RBM39 paralog that lacks an RRM3 domain but contains SR, RRM1, and RRM2 domains similar to RBM39. The RBM23 RRM2 domain has a high identity to the RBM39 RRM2. We found that RBM23 is recruited to the CRL4-DCAF15 E3 through a degron encompassing its RRM2 domain. Indisulam treatment leads to RBM23 degradation in a DCAF15-dependent, RBM39-independent manner. These results indicate that RBM23 is a bona fide neo-substrate targeted by aryl sulfonamides.

Past identification of neo-substrates has been successfully completed by various methods including *in vitro* ubiquitination of lysates, and proteomic analysis of ubiquitinated or total protein abundance following compound treatment (Iconomou and Saunders, 2016; Kronke et al., 2014). In addition to our studies of RBM23, we also attempted to identify neo-substrates through a more unbiased proteomics approach. In this approach, we sought to determine which proteins decrease in abundance with indisulam treatment and therefore might represent potential indisulam-dependent substrates. However, we were unable to identify any indisulam-dependent decreases in protein that were independent of RBM39 degradation (data not shown). In addition, with our depth of coverage, we were also unable to obtain spectral counts for RBM23. For this reason, we chose to utilize an alternative readout for detecting evidence of indisulam-mediated substrate degradation and downstream effects, which will be discussed in the next chapter.

Experimental Procedures

Endogenous Tagging in Cell Lines

For endogenous auxin-inducible-degron (AID) tagging, cells were first engineered to express the auxin-specific substrate receptor TIR1. For lentiviral expression of TIR1, 293T cells were seeded at 200,000 cells per well, and allowed to attach overnight. The next day, transfection complexes were prepared in 200 µL Opti-MEM and included 6 µL TransIT-Lenti (Mirus), 1 µg pLVX_TIR-V5-IRES-hygro, 100 ng pMD2.g (Addgene #12259), and 1 µg psPAX2 (Addgene #12260). Complexes were allowed to incubate at room temperature for 15 min, and added dropwise to the 293T cells. Lentivirus was collected and filtered 48 hr and 72 hr after transfection. Polybrene was added to the lentivirus at a final concentration of 8 µg/mL, and the lentivirus was used to infect the previously generated HCT116 RBM39-G269V cell line (Han et al., 2017). Three days after infection, the cells underwent selection with 500 µg/mL hygromycin for 7 days.

To generate the AID-tagged lines, the genomic region surrounding the RBM23 stop codon was targeted using three individual guide RNAs, which were each cloned into the px330 vector (Addgene #42230). Repair templates were cloned into the pGEM-T-Easy vector (Promega) and included an AID-3xFLAG tag, an IRES-Neo cassette flanked by LoxP sites, and 1 kB homology arms encoding regions upstream and downstream of the stop codon. Repair templates included the last intron directly before the stop codon. HCT116 RBM39-G268V TIR1-expressing cell line were transfected with 1 µg repair template and 500 ng of mastermix containing equal amounts of the three RBM23 guides. Cells underwent selection with 1 mg/ml G418, and individual clones were isolated. Integration of the tags was

validated by western blot using FLAG-HRP antibody (1:3000, Sigma-Aldrich). Clones with homozygous integration of the AID-FLAG tag were identified through PCR analysis using the following primers: 5' CCTCAGTGAGCATACAATTTTCC 3' and 5'CCAGGTGTGAGTTTTCATTTTTC 3'. Homozygously-tagged clones were then subjected to dose responses with indisulam and IAA, and evaluated by western blot for TIR1-V5 expression and RBM23 degradation using V5-HRP antibody (Sigma-Aldrich) and FLAG-HRP antibody (Sigma-Aldrich), respectively. Clones were then further validated by Sanger sequencing.

To generate the RBM23-3xFLAG endogenously-tagged lines, the genomic region surrounding the RBM23 stop codon was targeted using three individual guide RNAs, which were each cloned into the px330 vector. Templates were cloned into the pGEM-T-Easy vector and included a 3xFLAG tag, an IRES-Neo cassette flanked by LoxP sites, and 1 kB homology arms encoding regions upstream and downstream of the stop codon. Repair templates did not include the last intron directly before the stop codon. The HCT116 parental cell line was transfected with 1 μg repair template and 500 ng of mastermix containing equal amounts of the three RBM23 guides. Cells underwent selection with 1 mg/ml G418, and individual clones were isolated. Integration of the tags was validated by western blot using FLAG-HRP antibody. Clones expressing the tag were identified through PCR analysis using the following primers: 5'-CCTCAGTGAGCATACAATTTTCC-3' and 5'-CCAGGTGTGAGTTTTCATTTTTC-3'. Clones were then further validated by Sanger sequencing.

For expression of DCAF15 CRISPR guides, the following DCAF15 guide was cloned into LentiCRISPRv2 (Addgene #52961): CGTGTCCCTCAAGAACATTG. Lentivirus was generated by transfecting 293T cells with a mixture containing 200 µL Opti-MEM, LentiCRISPRv2 sgDCAF15 plasmid and lentiviral packaging plasmids. Lentivirus was then used to infect the HCT-116 RBM23-3xFLAG cell line. Cells were selected with 2 µg/ml puromycin for 7 days.

Indisulam-dependent Degradation Assays

For monitoring indisulam-dependent degradation of mutants, RBM39 and RBM23 sequences were cloned into the pcDNA3.1+ vector and tagged with a C-terminal HA tag. 293Ts were seeded in a 6-well plate at 0.5 million cells per well one day prior to transfection. For each well, TransIT:DNA complexes were prepared by combining 200 µL Opti-MEM, 3 µL TransIT-LT1 (Mirus), and 1 µg of DNA (200 ng pcDNA3-RBM23-HA or pcDNA3-RBM39-HA, 400 ng pcDNA3-DCAF15-3xFLAG, 350 ng pcDNA3-3xFLAG, and 50 ng pmaxGFP). Complexes were allowed to incubate at room temperature for 15 min, and then added dropwise to 293T cells. Forty-eight hours after transfection, cells were treated with the indicated doses of indisulam or indoleacetic acid (IAA). Cells were lysed in 1% SDS, with benzonase (Sigma) diluted 1:10,000 in Buffer A (50 mM HEPES 7.4, 10 mM KCl, and 2 mM MgCl2). Samples were analyzed by western blot using HA-HRP antibody (1:3000, 6E2, Cell Signaling Technology) and FLAG-HRP antibody (1:3000, Clone M2, Sigma-Aldrich).

Recombinant Protein Expression and Purification

To generate recombinant protein for FRET assays, RBM39 amino acids 250-330 or RBM23 amino acids 210-330 were tagged with an N-terminal 6xHis tag and C-terminal 3xFLAG tag. Constructs were transformed into Escherichia coli BL21(DE3), and cultures were grown at 37°C to an OD600 of 0.6-0.8. IPTG was added to a final concentration of 0.4 mM, and the cultures were incubated overnight at 16°C. Bacteria was pelleted and lysed in a buffer containing 40 mM Tris (pH 7.5), 225 mM NaCl, 1mM TCEP, and 1x SigmaFAST protease inhibitors. Cell suspension was sonicated, centrifuged at 35000 rpm for 30 min, filtered, and incubated with Ni-NTA agarose (QIAGEN) for 2h with rotation at 4°C. Beads were washed three times with wash buffer (40 mM Tris, 225 mM NaCl, 1 mM TCEP, 20 mM imidazole, pH 7.5) and eluted with elution buffer (40 mM Tris, 225 mM NaCl, 1 mM TCEP, 300 mM imidazole, pH 7.5). His tags were removed by overnight cleavage at 4°C with TEV protease. Cleaved proteins were incubated with nickel-NTA resin to remove cleaved His tags, and further purified by size-exclusion chromatography using a Superdex200 Increase 10/300 column (GE Healthcare). The protein eluted at 18-19 mL, and was stored at 80°C in 40 mM Tris, 225 mM NaCl, 1 mM TCEP, pH 7.5.

TR-FRET Assays

TR-FRET reactions were performed in triplicate in a 384-well plate at a final volume of 10 µL/well. Final assay concentrations were the following: 5 ng/µL anti-FLAG M2-XL665 (CisBio), 1 nM anti-6xHis LANCE Eu-W1024 (Perkin Elmer), 0.1 µM $RBM39_{250-330}$-3xFLAG or $RBM23_{210-330}$-3xFLAG protein, and 0.1 µM His-DCAF15/DDB1/DDA1

complex. Reactions were carried out in 25 mM HEPES pH 7.4, 100 mM NaCl, 0.1 mg/ml BSA, 0.005% Tween, and 0.5 mM TCEP. Samples were treated with DMSO or indisulam, incubated 5 min at room temperature, and read using a Cytation 5 instrument (Biotek). The Eu-labeled donor was excited at 360 nm, and its emission was monitored at 620 nm. Emission of the XL665-labeled acceptor was monitored at 665 nm. The TR-FRET ratio was calculated as the signal at 665 nm divided by the signal at 620 nm, and plotted as the mean ± SEM. The EC_{50} was calculated from a four parameter dose-response curve generated with the Prism 8 software package.

CHAPTER SIX: CHARACTERIZATION OF CELLULAR CONSEQUENCES OF INDISULAM TREATMENT

Introduction

RBM39 and RBM23 have previously been reported to regulate transcriptional activation and alternative splicing, but their distinct roles in these processes have not been clearly defined (Dowhan et al., 2005). We previously demonstrated that indisulam causes splicing defects by degrading RBM39 (Han et al., 2017). We reasoned that indisulam would also cause changes in gene expression and possibly splicing as a result of degradation of RBM23 and perhaps yet unidentified substrates. Previous data from our lab suggest that RBM39 is an essential gene since our attempts to genetically ablate RBM39 in multiple cancer cell lines were unsuccessful (data not shown). However, RBM23 does not appear to share this essential function as it can be readily deleted from cell lines (data not shown). We sought to determine which targets may differ between the two RNA binding proteins and therefore may be the cause of decreased cell viability with RBM39 degradation. In addition, RBM39 and RBM23 have similar RRM2 sequences which presumably target RNA. However, RBM39 and RBM23 have different SR domains, which suggests that they may interact with unique sets of protein partners, leading to differential splicing effects. Therefore, we proposed to compare splicing changes dependent on these two proteins and any other yet undiscovered substrates to gain insight on their functions and downstream effects (Figure 6-1).

Indisulam-Mediated Changes in Differential Gene Expression are Dependent on RBM39

We developed an isogenic system to assay gene expression and splicing changes that are the consequence of RBM39, RBM23, and any other putative substrates (Figure 6-2A). The first cell line (cell line #1) is an HCT-116 cell line that expresses wild type RBM39 and a 3XFLAG-tagged RBM23. We tested indisulam treatment in this cell line and observed that RBM39 was degraded, as expected (Figure 6-2B). The second cell line is an HCT-116 cell line with RBM39 G268V in which we used CRISPR/Cas9 to engineer an Auxin-Inducible Degron (AID) and 3XFLAG epitope into the C-terminus of both alleles of RBM23. The latter cell line also expresses the plant E3 ubiquitin ligase TIR1, so that in the presence of indoleacetic acid (IAA), RBM23-AID-3XFLAG is recruited to TIR1 and degraded (Figure 6-2C). We used massively parallel RNA sequencing to compare gene expression changes for each cell line following 12-hour treatment with DMSO, 10 μM indisulam, or 100 μM IAA. Using this system, we can identify changes in gene expression or splicing that are specific to either RBM39, RBM23, or as yet an unknown indisulam neo-substrate.

Indisulam treatment altered expression of 3080 genes (Figure 6-3A). By contrast, we found no significant gene expression changes in RBM39 G268V cells (Figure 6-3A). This observation suggests that RBM23 and any yet unidentified substrate have no impact on gene expression 12 hours following 10 μM of indisulam. To confirm that RBM23 had no impact on gene expression, we used IAA to selectively degrade RBM23 to even lower levels than with indisulam-mediated degradation (Figure 6-2C). IAA treatment alone in a cell line without AID-tagged proteins did not lead to any gene expression changes (Figure 6-3A).

IAA-induced RBM23 degradation also did not result in any gene expression changes, suggesting that RBM23 has minimal to no impact on gene expression in HCT-116 cells (Figure 6-3A). Taken together, we concluded that all of the gene expression changes that we identified following indisulam treatment are due to RBM39 degradation.

Indisulam-Mediated Changes in Splicing are Dependent on RBM39

Similar to our gene expression analysis, indisulam treatment resulted in multiple splicing events that were all dependent on RBM39. Indisulam treatment for 12 hrs resulted in 1640 exon-skipping events, 132 intron retention events, and 22 alternative splice site events (Fig 6-3B). However, no RBM39-independent splicing changes occurred following indisulam treatment in cells expressing the RBM39 G268V allele. In addition, no RBM23-dependent splicing events were detected following auxin treatment in the RBM23-AID cell line (Fig 6-3B). Taken together, these results suggest that the observed effect of indisulam on splicing is mediated exclusively through RBM39 and not through degradation of RBM23 or any other substrate.

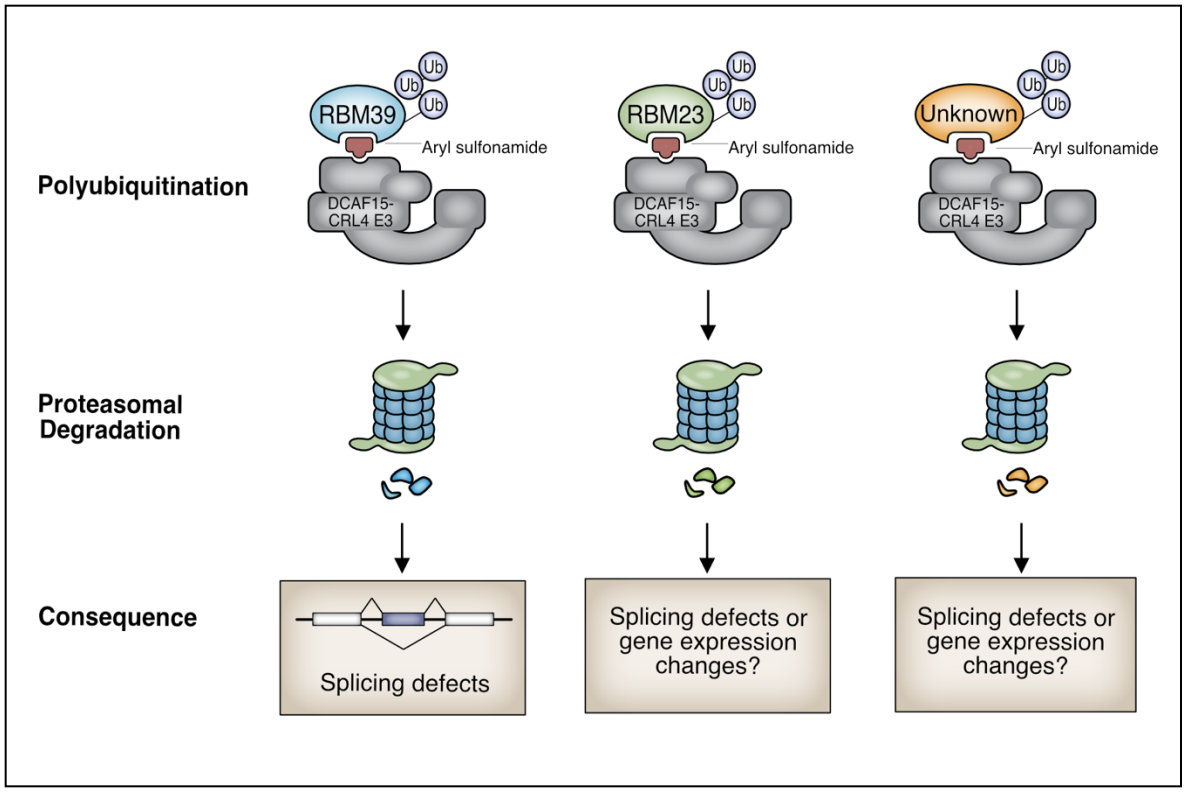

Figure 6-1. Schematic outline for identifying cellular consequences of aryl sulfonamide-mediated substrate degradation.

The goal of this project was to utilize RNA sequencing to monitor the effects of sulfonamide-mediated degradation of RBM39, RBM23, or another yet unknown substrate.

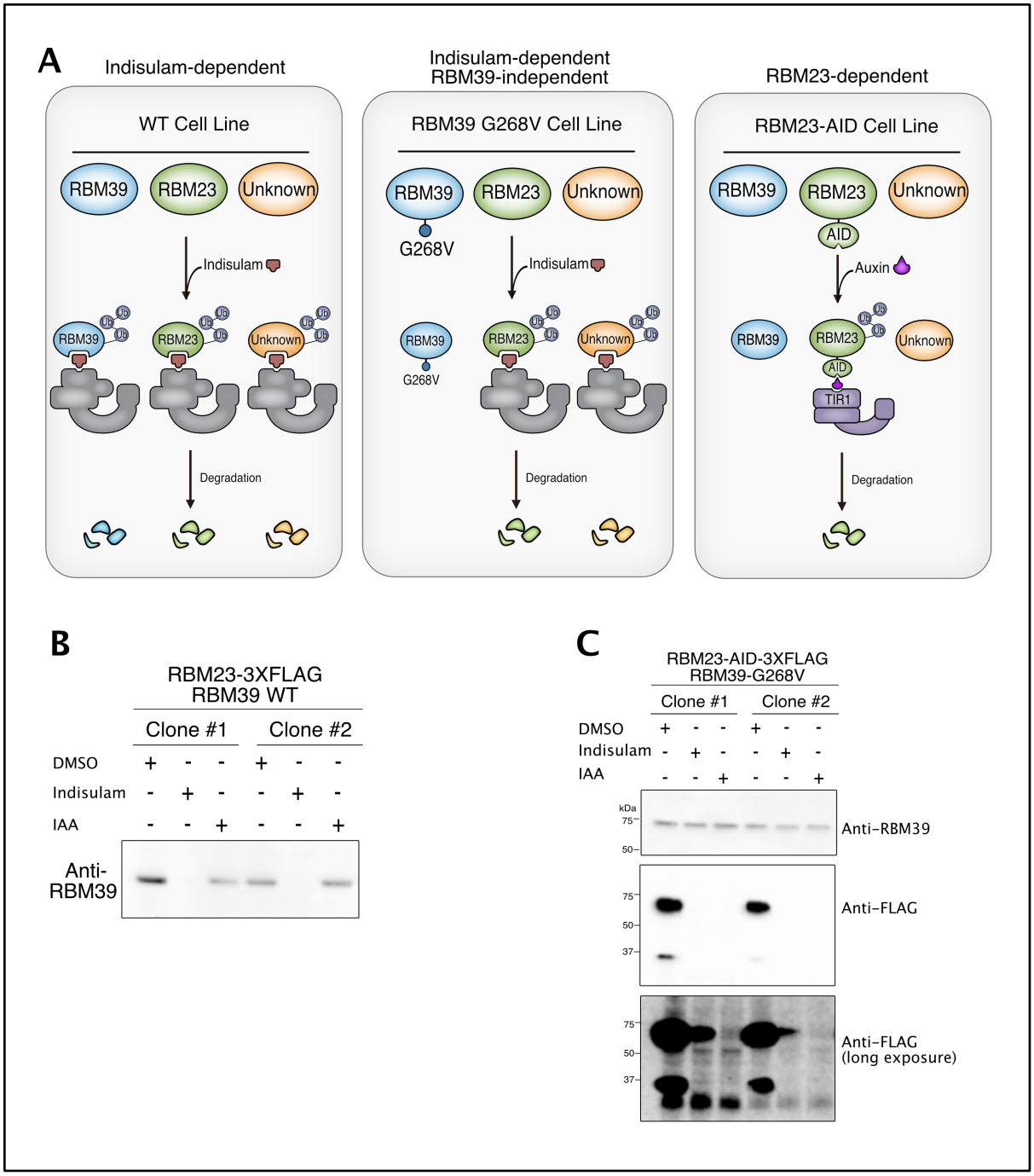
A
Indisulam-dependent
WT Cell Line
RBM39
RBM23
Unknown
Indisulam
Degradation
Indisulam-dependent
RBM39-independent
RBM39 G268V Cell Line
G268V
RBM23-dependent
RBM23-AID Cell Line
AID
Auxin
TIR1
B
RBM23-3XFLAG
RBM39 WT
Clone #1
Clone #2
DMSO
Indisulam
IAA
Anti-
RBM39
C
RBM23-AID-3XFLAG
RBM39-G268V
kDa
75
50
37
Anti-RBM39
Anti-FLAG
Anti-FLAG
(long exposure)

Figure 6-2. Experimental conditions for examining the effects of substrate degradation.

(A) Schematic diagram of cell lines used to examine RNA expression and splicing. Endogenously-tagged RBM23 cell lines in the background of wild-type RBM39 or RBM39 G268V were treated with DMSO, indisulam (10 μM), or IAA (100 μM) for 12 h. Two clones per cell line were used for gene expression analysis. (B) Validation of the wild-type RBM39 cell line. RBM39 degrades with indisulam treatment in the endogenously tagged RBM23-3xFLAG; RBM39 WT cell line. Samples were treated with DMSO, 10 μM indisulam, or 100 μM IAA for 12 hrs. Samples were then collected for RNA purification and western blot analyses. (C) Validation of the endogenously-tagged RBM23-AID-3xFLAG cell line. Tagged RBM23 is degraded with indisulam or IAA treatment. Cells were treated using the conditions outlined in Figure 6-2B, and analyzed by western blotting with FLAG-HRP antibody.

A

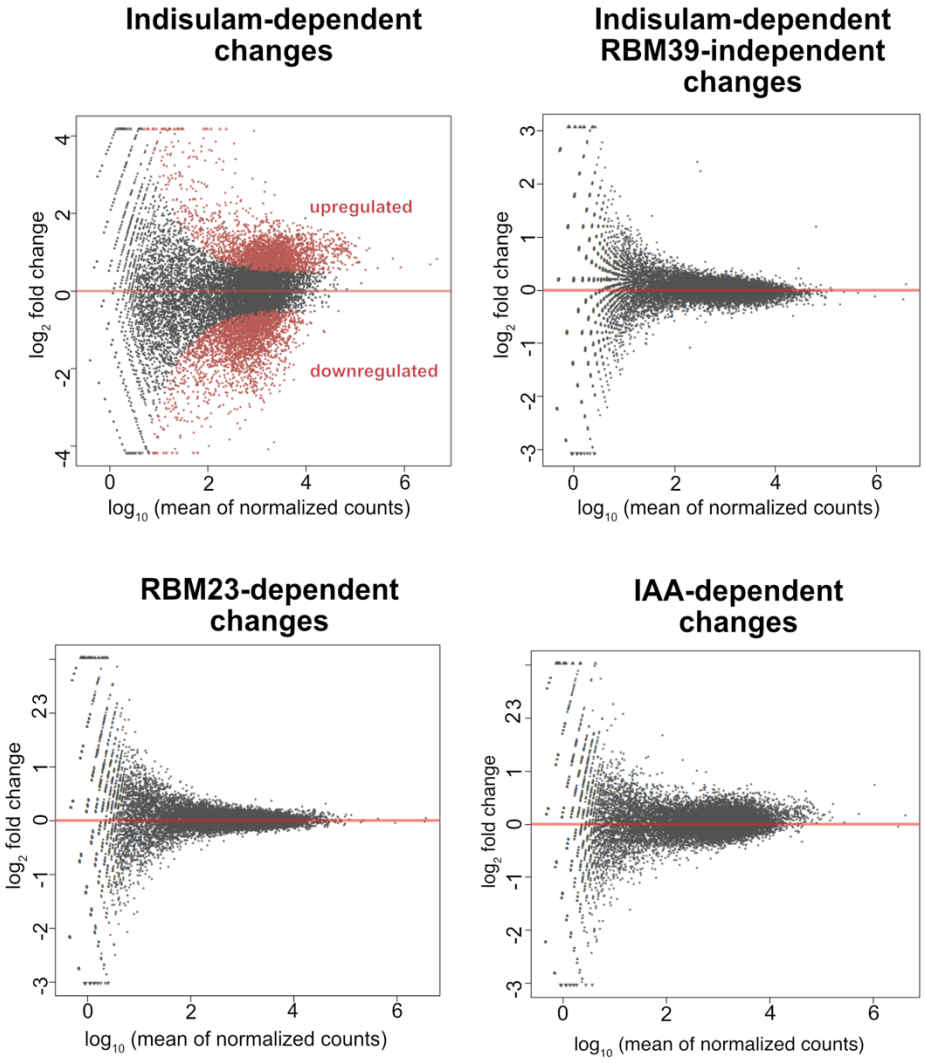

B

	Indisulam-dependent changes	Indisulam-dependent RBM39-independent changes	RBM23-dependent changes
Exon skipping	1640	0	0
Exon inclusion	11	0	0
Intron skipping	8	0	0
Intron retention	132	0	0
Alternative 5' splice site	10	0	0
Alternative 3' splice site	12	0	0

Figure 6-3. Indisulam-mediated gene expression and splicing changes are dependent on RBM39.

(A) MA plots of indisulam-specific, RBM39-specific, RBM23-specific, and auxin-specific changes in differential gene expression. Upregulated or downregulated genes with each condition are indicated in red ($p < 0.05$, $\log_2$ fold change > 1). (B) Table of splicing events that are dependent on indisulam, RBM39, or RBM23. Treatment with indisulam leads to exon skipping and intron retention events that are dependent on RBM39 degradation.

Discussion

RBM39 belongs to a large family of more than 450 RNA-binding proteins (RBPs) with diverse roles in human disease (Dvinge et al., 2016; Lee and Abdel-Wahab, 2016; Wang et al., 2019). RBPs traditionally have a modular structure consisting of multiple RNA-binding domains including RNA-recognition motifs (RRMs) or K-homology (KH) domains (Burd and Dreyfuss, 1994; Lunde et al., 2007). RBPs have been shown to be key regulators of gene expression and are implicated in many disease processes including cancer and neurodegeneration (Cooper et al., 2009). Small molecules that degrade specific RBPs would have multiple potential clinical applications, and thus there is enthusiasm for using sulfonamide derivatives to target RBP neo-substrates other than RBM39.

A key question for drug development is whether sulfonamide derivatives can be used to target a variety of different RNA binding proteins (RBPs) containing RRM domains, much like IMiDs target transcription factors with zinc finger domains (Petzold et al., 2016; Sievers et al., 2018). Here, we built an isogenic system to test the hypothesis that indisulam may modulate levels of other RNA-binding proteins (RBPs) in addition to RBM39. We then used this system to monitor any effects of indisulam treatment via RNA sequencing analyses. We expected that cells with RBM39 mutations that prevent RBM39 interaction with the CRL4-DCAF15 E3 might still exhibit gene expression changes that are the result of degradation of RBM23 or other yet undefined substrates. Strikingly, we found that gene expression was essentially unchanged in cells that cannot degrade RBM39. At this depth of coverage, it is possible that our analysis did not detect rare transcripts influenced by other substrates. Notwithstanding, we concluded that RBM23 is not essential for proliferation of HCT-116

cells and has minimal impact on gene expression or splicing. Furthermore, we found no gene expression or splicing changes that might be explained by an alternative neo-substrate. The absence of any gene expression changes in RBM39 G268V cells suggests that indisulam may be remarkably selective for RBM39 and RBM23, in contrast to the relatively promiscuous recognition of substrates by IMiD molecular glues.

Experimental Procedures

RNA Sequencing and Bioinformatic Analysis of Splicing Events

RNA sequencing analysis was performed in HCT116 cell lines in which RBM23 was endogenously tagged with 3xFLAG or AID-3xFLAG at the C-terminus. In brief, cells were treated with DMSO, 10 μM indisulam, or 100 μM IAA for 12 hours. RNA was extracted using the Quick-RNA MiniPrep kit (Zymo) and treated with TURBO DNase (Ambion) to remove genomic DNA. Following mRNA enrichment, cDNA libraries were generated using the TruSeq Stranded mRNA Sample Prep Kit (Illumina). Strand-specific single-end RNA sequencing was performed using Illumina NextSeq. The quality of the sequencing reads was evaluated using NGS QC Toolkit (v2.3.3) (Patel and Jain, 2012) and high-quality reads were extracted. The data files of the reference genome, hg19, were downloaded from Illumina iGenomes (https://support.illumina.com/sequencing/sequencing_software/igenome.html). The quality of the RNA-sequencing libraries was estimated by mapping the reads onto human transcript and ribosomal RNA sequences (Ensembl release 89) using Bowtie (v2.3.2) (Langmead and Salzberg, 2012). STAR(Dobin et al., 2013) was employed to align the reads onto the reference genome and HTSeq Python package (Anders et al., 2015) was employed to count reads per gene. DESeq R Bioconductor package (Anders and Huber, 2010; Gentleman et al., 2004) was used to normalize read counts and identify differentially expressed (DE) genes. KEGG (Kanehisa et al., 2017) pathway data was downloaded using KEGG API (https://www.kegg.jp/kegg/rest/keggapi.html) and gene ontology (GO) data was

downloaded from NCBI FTP (ftp://ftp.ncbi.nlm.nih.gov/gene/DATA/gene2go.gz). The enrichment of DE genes to pathways and GOs were calculated by Fisher's exact test in R statistical package. Differential alternative splicing events were identified using SpliceFisher (https://github.com/jiwoongbio/SpliceFisher).

Quantification and Statistical Analysis

DCAF15 mutagenesis sequencing data was analyzed using the NGS QC Toolkit (v2.3.3), Burrows-Wheler Aligner (BWA, v0.7.15a), and SAMtools. Significance was calculated by Fisher's exact test. For RNA sequencing analyses, data was analyzed using NGS QC Toolkit (v2.3.3), Bowtie (v2.23.2), HTSeq python package, and DESeq R Bioconductor package. Significance was calculated by Fisher's exact test. For FRET assays, experiments were performed in triplicate and plotted as mean ± SEM. The EC50 was calculated from a four parameter dose response curve generated with the Prism 8 software package.

CHAPTER 7: CONCLUSION

The discovery of molecular glue degraders like IMiDs and sulfonamides represents a seminal breakthrough in drug development by targeting conventionally undruggable proteins that lack well-defined binding pockets. With the discovery of multiple IMiD targets, there has been great interest in determining whether indisulam and related sulfonamides can also be harnessed to degrade a diverse range of substrates. The overarching goal of the work presented here was to broaden our understanding of molecular glue targets and the principles governing their degradation. Specifically, we sought to elucidate the molecular mechanisms for RBM39 recruitment and ubiquitination by the CRL4-DCAF15 E3, and to apply this knowledge toward discovery of novel endogenous substrates and neo-substrates.

Using a combination of biochemical and cellular assays, our results demonstrate that the CRL4-DCAF15 E3 ligase is sufficient for sulfonamide-dependent neo-substrate ubiquitination. Structure-function studies of the complex revealed the RRM2 domain of RBM39 as both necessary and sufficient for compound-dependent recruitment to CRL4-DCAF15. These observations are consistent with our prior studies in which we identified mutations in the RRM2 that render RBM39 resistant to sulfonamide-mediated degradation (Han et al., 2017). We have also determined that the preferred sites for RBM39 ubiquitination are lysine residues located in an N-terminal region. Having defined the regions necessary for RBM39 recruitment and ubiquitination, we also sought to discover other potential neo-substrates with similar features. We identified RBM23 as

another neo-substrate that is ubiquitinated by the CRL4-DCAF15 E3 ligase. The RBM23 RRM2 domain has a high sequence identity to the RBM39 RRM2 degron sequence. We found that RBM23 is also recruited to the CRL4-DCAF15 E3 ligase via a region encompassing its RRM2 domain, and is able to undergo sulfonamide-dependent degradation independent of RBM39 degradation.

Using an RNA sequencing-based approach, we sought to monitor direct or downstream effects of indisulam-dependent substrate degradation. In these experiments, we examined sulfonamide-dependent gene expression changes in cell lines with mutations that prevent RBM39 degradation. Using these cell lines, we sought to monitor gene expression changes that are the result of degradation of RBM23 or other yet undefined substrates. We found that gene expression and splicing were unchanged in cells that are unable to degrade RBM39. Our conclusion from these experiments was that indisulam mediates its effects through RBM39 degradation, and not through degradation of other neo-substrates. These results suggest that indisulam may be more selective for fewer substrates than originally hypothesized, in contrast to the promiscuous targeting of multiple substrates by IMiD molecular glues.

Structural studies have highlighted the differences between IMiD and aryl sulfonamide molecule glues, and have clearly defined the mechanism of action for indisulam (Bussiere et al., 2020; Du et al., 2019; Faust et al., 2020). Prior to the work of these structural biologists, it was uncertain whether indisulam exerts its effects allosterically by binding to either DCAF15 or RBM39, or whether indisulam acts as a molecular glue to bridge the interaction between RBM39 and DCAF15. Structural

analysis of the DDB1-DDA1-DCAF15-indisulam-RBM39(RRM2) complex revealed that indisulam acts as a molecular glue by occupying a shallow binding pocket in DCAF15 and forming contacts with both DCAF15 and RBM39. In addition, DCAF15 and RBM39 also form weak contacts to stabilize the formation of this ternary complex. Previous structural work demonstrated that IMiDs occupy a highly conserved binding pocket on the substrate receptor cereblon, which may suggest that a natural ligand is recruited to this site. In contrast, the binding pocket in DCAF15 is not highly conserved, suggesting that any endogenous substrates for the CRL4-DCAF15 E3 may be recruited to another site. DCAF15 was found to have a unique structural conformation that is distinct from other CRL4 substrate receptors. In addition, the DCAF15-sulfonamide-RBM39 complex forms more substantial interactions than the CRBN-IMiD-zinc finger complexes, which may result in increased specificity of DCAF15 for a small number of substrates. In contrast to the high affinity interaction between IMiDs and the CRBN receptor, aryl sulfonamides have a very weak affinity for DCAF15 in the absence of RBM39. Although hundreds of RRM-containing proteins exist, these structural studies support the hypothesis that only a limited number of substrates contain the specific critical residues required for interaction with sulfonamides and DCAF15, leading to a much higher specificity than originally predicted.

Indisulam and related aryl sulfonamides are promising therapies, particularly for hematopoietic cancers dependent on RNA binding protein (RBP) function. Our work presented herein contributes to our knowledge of the principles governing sulfonamide-mediated targeting of substrates. Lessons from studies of both IMiDs and aryl

sulfonamides are likely to guide their clinical application and lead to discovery of additional molecular glues for therapeutic use.

BIBLIOGRAPHY

1. Agopiantz, M., Corbonnois, P., Sorlin, A., Bonnet, C., Klein, M., Hubert, N., Pascal-Vigneron, V., Jonveaux, P., Cuny, T., Leheup, B.*, et al.* (2014). Endocrine disorders in Woodhouse-Sakati syndrome: a systematic review of the literature. J Endocrinol Invest *37*, 1-7.
2. Alazami, A.M., Al-Saif, A., Al-Semari, A., Bohlega, S., Zlitni, S., Alzahrani, F., Bavi, P., Kaya, N., Colak, D., Khalak, H.*, et al.* (2008). Mutations in C2orf37, encoding a nucleolar protein, cause hypogonadism, alopecia, diabetes mellitus, mental retardation, and extrapyramidal syndrome. Am J Hum Genet *83*, 684-691.
3. Ali, A., Mistry, B.V., Ahmed, H.A., Abdulla, R., Amer, H.A., Prince, A., Alazami, A.M., Alkuraya, F.S., and Assiri, A. (2018). Deletion of DDB1- and CUL4-associated factor-17 (Dcaf17) gene causes spermatogenesis defects and male infertility in mice. Sci Rep *8*, 9202.
4. Anders, S., and Huber, W. (2010). Differential expression analysis for sequence count data. Genome Biol *11*, R106.
5. Anders, S., Pyl, P.T., and Huber, W. (2015). HTSeq--a Python framework to work with high-throughput sequencing data. Bioinformatics *31*, 166-169.
6. Andtbacka, R.H., Kaufman, H.L., Collichio, F., Amatruda, T., Senzer, N., Chesney, J., Delman, K.A., Spitler, L.E., Puzanov, I., Agarwala, S.S.*, et al.* (2015).

Talimogene Laherparepvec Improves Durable Response Rate in Patients With Advanced Melanoma. J Clin Oncol *33*, 2780-2788.

7. Baek, K., and Schulman, B.A. (2020). Molecular glue concept solidifies. Nat Chem Biol *16*, 2-3.
8. Bhuripanyo, K., Wang, Y., Liu, X., Zhou, L., Liu, R., Duong, D., Zhao, B., Bi, Y., Zhou, H., Chen, G.*, et al.* (2018). Identifying the substrate proteins of U-box E3s E4B and CHIP by orthogonal ubiquitin transfer. Sci Adv *4*, e1701393.
9. Bondeson, D.P., Mares, A., Smith, I.E., Ko, E., Campos, S., Miah, A.H., Mulholland, K.E., Routly, N., Buckley, D.L., Gustafson, J.L.*, et al.* (2015). Catalytic in vivo protein knockdown by small-molecule PROTACs. Nat Chem Biol *11*, 611-617.
10. Brunet, J.F., Denizot, F., Luciani, M.F., Roux-Dosseto, M., Suzan, M., Mattei, M.G., and Golstein, P. (1987). A new member of the immunoglobulin superfamily--CTLA-4. Nature *328*, 267-270.
11. Burd, C.G., and Dreyfuss, G. (1994). Conserved structures and diversity of functions of RNA-binding proteins. Science *265*, 615-621.
12. Burslem, G.M., and Crews, C.M. (2020). Proteolysis-Targeting Chimeras as Therapeutics and Tools for Biological Discovery. Cell *181*, 102-114.
13. Burslem, G.M., Smith, B.E., Lai, A.C., Jaime-Figueroa, S., McQuaid, D.C., Bondeson, D.P., Toure, M., Dong, H., Qian, Y., Wang, J.*, et al.* (2018). The Advantages of Targeted Protein Degradation Over Inhibition: An RTK Case Study. Cell Chem Biol *25*, 67-77 e63.

14. Bussiere, D.E., Xie, L., Srinivas, H., Shu, W., Burke, A., Be, C., Zhao, J., Godbole, A., King, D., Karki, R.G.*, et al.* (2020). Structural basis of indisulam-mediated RBM39 recruitment to DCAF15 E3 ligase complex. Nat Chem Biol *16*, 15-23.

15. Cavadini, S., Fischer, E.S., Bunker, R.D., Potenza, A., Lingaraju, G.M., Goldie, K.N., Mohamed, W.I., Faty, M., Petzold, G., Beckwith, R.E.*, et al.* (2016). Cullin-RING ubiquitin E3 ligase regulation by the COP9 signalosome. Nature *531*, 598-603.

16. Chamberlain, P.P., and Hamann, L.G. (2019). Development of targeted protein degradation therapeutics. Nat Chem Biol *15*, 937-944.

17. Chamberlain, P.P., Lopez-Girona, A., Miller, K., Carmel, G., Pagarigan, B., Chie-Leon, B., Rychak, E., Corral, L.G., Ren, Y.J., Wang, M.*, et al.* (2014). Structure of the human Cereblon-DDB1-lenalidomide complex reveals basis for responsiveness to thalidomide analogs. Nat Struct Mol Biol *21*, 803-809.

18. Che, Y., Gilbert, A.M., Shanmugasundaram, V., and Noe, M.C. (2018). Inducing protein-protein interactions with molecular glues. Bioorg Med Chem Lett *28*, 2585-2592.

19. Cooper, T.A., Wan, L., and Dreyfuss, G. (2009). RNA and disease. Cell *136*, 777-793.

20. Dang, C.V., Reddy, E.P., Shokat, K.M., and Soucek, L. (2017). Drugging the 'undruggable' cancer targets. Nat Rev Cancer *17*, 502-508.

21. Deckert, M., Elly, C., Altman, A., and Liu, Y.C. (1998). Coordinated regulation of the tyrosine phosphorylation of Cbl by Fyn and Syk tyrosine kinases. J Biol Chem *273*, 8867-8874.

22. Deshaies, R.J. (2015). Protein degradation: Prime time for PROTACs. Nat Chem Biol *11*, 634-635.

23. Dittrich, C., Dumez, H., Calvert, H., Hanauske, A., Faber, M., Wanders, J., Yule, M., Ravic, M., and Fumoleau, P. (2003). Phase I and pharmacokinetic study of E7070, a chloroindolyl-sulfonamide anticancer agent, administered on a weekly schedule to patients with solid tumors. Clin Cancer Res *9*, 5195-5204.

24. Dobin, A., Davis, C.A., Schlesinger, F., Drenkow, J., Zaleski, C., Jha, S., Batut, P., Chaisson, M., and Gingeras, T.R. (2013). STAR: ultrafast universal RNA-seq aligner. Bioinformatics *29*, 15-21.

25. Donovan, K.A., An, J., Nowak, R.P., Yuan, J.C., Fink, E.C., Berry, B.C., Ebert, B.L., and Fischer, E.S. (2018). Thalidomide promotes degradation of SALL4, a transcription factor implicated in Duane Radial Ray syndrome. Elife *7*.

26. Douglass, E.F., Jr., Miller, C.J., Sparer, G., Shapiro, H., and Spiegel, D.A. (2013). A comprehensive mathematical model for three-body binding equilibria. J Am Chem Soc *135*, 6092-6099.

27. Dowhan, D.H., Hong, E.P., Auboeuf, D., Dennis, A.P., Wilson, M.M., Berget, S.M., and O'Malley, B.W. (2005). Steroid hormone receptor coactivation and alternative RNA splicing by U2AF65-related proteins CAPERalpha and CAPERbeta. Mol Cell *17*, 429-439.

28. Druker, B.J., Tamura, S., Buchdunger, E., Ohno, S., Segal, G.M., Fanning, S., Zimmermann, J., and Lydon, N.B. (1996). Effects of a selective inhibitor of the Abl tyrosine kinase on the growth of Bcr-Abl positive cells. Nat Med *2*, 561-566.

29. Du, X., Volkov, O.A., Czerwinski, R.M., Tan, H., Huerta, C., Morton, E.R., Rizzi, J.P., Wehn, P.M., Xu, R., Nijhawan, D.*, et al.* (2019). Structural Basis and Kinetic Pathway of RBM39 Recruitment to DCAF15 by a Sulfonamide Molecular Glue E7820. Structure *27*, 1625-1633 e1623.

30. Duda, D.M., Borg, L.A., Scott, D.C., Hunt, H.W., Hammel, M., and Schulman, B.A. (2008). Structural insights into NEDD8 activation of cullin-RING ligases: conformational control of conjugation. Cell *134*, 995-1006.

31. Dvinge, H., Kim, E., Abdel-Wahab, O., and Bradley, R.K. (2016). RNA splicing factors as oncoproteins and tumour suppressors. Nat Rev Cancer *16*, 413-430.

32. Enchev, R.I., Schulman, B.A., and Peter, M. (2015). Protein neddylation: beyond cullin-RING ligases. Nat Rev Mol Cell Biol *16*, 30-44.

33. Eshhar, Z., Waks, T., Gross, G., and Schindler, D.G. (1993). Specific activation and targeting of cytotoxic lymphocytes through chimeric single chains consisting of antibody-binding domains and the gamma or zeta subunits of the immunoglobulin and T-cell receptors. Proc Natl Acad Sci U S A *90*, 720-724.

34. Faust, T.B., Yoon, H., Nowak, R.P., Donovan, K.A., Li, Z., Cai, Q., Eleuteri, N.A., Zhang, T., Gray, N.S., and Fischer, E.S. (2020). Structural complementarity facilitates E7820-mediated degradation of RBM39 by DCAF15. Nat Chem Biol *16*, 7-14.

35. Fischer, E.S., Bohm, K., Lydeard, J.R., Yang, H., Stadler, M.B., Cavadini, S., Nagel, J., Serluca, F., Acker, V., Lingaraju, G.M.*, et al.* (2014). Structure of the DDB1-CRBN E3 ubiquitin ligase in complex with thalidomide. Nature *512*, 49-53.

36. Fisher, S.L., and Phillips, A.J. (2018). Targeted protein degradation and the enzymology of degraders. Curr Opin Chem Biol *44*, 47-55.

37. Flick, K., Ouni, I., Wohlschlegel, J.A., Capati, C., McDonald, W.H., Yates, J.R., and Kaiser, P. (2004). Proteolysis-independent regulation of the transcription factor Met4 by a single Lys 48-linked ubiquitin chain. Nat Cell Biol *6*, 634-641.

38. Fukuoka, K., Usuda, J., Iwamoto, Y., Fukumoto, H., Nakamura, T., Yoneda, T., Narita, N., Saijo, N., and Nishio, K. (2001). Mechanisms of action of the novel sulfonamide anticancer agent E7070 on cell cycle progression in human non-small cell lung cancer cells. Invest New Drugs *19*, 219-227.

39. Gentleman, R.C., Carey, V.J., Bates, D.M., Bolstad, B., Dettling, M., Dudoit, S., Ellis, B., Gautier, L., Ge, Y., Gentry, J.*, et al.* (2004). Bioconductor: open software development for computational biology and bioinformatics. Genome Biol *5*, R80.

40. Groffen, J., Stephenson, J.R., Heisterkamp, N., de Klein, A., Bartram, C.R., and Grosveld, G. (1984). Philadelphia chromosomal breakpoints are clustered within a limited region, bcr, on chromosome 22. Cell *36*, 93-99.

41. Guharoy, M., Bhowmick, P., Sallam, M., and Tompa, P. (2016). Tripartite degrons confer diversity and specificity on regulated protein degradation in the ubiquitin-proteasome system. Nat Commun *7*, 10239.

42. Haddad, R.I., Weinstein, L.J., Wieczorek, T.J., Bhattacharya, N., Raftopoulos, H., Oster, M.W., Zhang, X., Latham, V.M., Jr., Costello, R., Faucher, J.*, et al.* (2004). A phase II clinical and pharmacodynamic study of E7070 in patients with metastatic, recurrent, or refractory squamous cell carcinoma of the head and neck: modulation of retinoblastoma protein phosphorylation by a novel chloroindolyl sulfonamide cell cycle inhibitor. Clin Cancer Res *10*, 4680-4687.

43. Han, T., Goralski, M., Gaskill, N., Capota, E., Kim, J., Ting, T.C., Xie, Y., Williams, N.S., and Nijhawan, D. (2017). Anticancer sulfonamides target splicing by inducing RBM39 degradation via recruitment to DCAF15. Science *356*.

44. Hannah, J., and Zhou, P. (2015). Distinct and overlapping functions of the cullin E3 ligase scaffolding proteins CUL4A and CUL4B. Gene *573*, 33-45.

45. Hanson, S.M., Georghiou, G., Thakur, M.K., Miller, W.T., Rest, J.S., Chodera, J.D., and Seeliger, M.A. (2019). What Makes a Kinase Promiscuous for Inhibitors? Cell Chem Biol *26*, 390-399 e395.

46. Heisterkamp, N., Stephenson, J.R., Groffen, J., Hansen, P.F., de Klein, A., Bartram, C.R., and Grosveld, G. (1983). Localization of the c-ab1 oncogene adjacent to a translocation break point in chronic myelocytic leukaemia. Nature *306*, 239-242.

47. Hines, J., Lartigue, S., Dong, H., Qian, Y., and Crews, C.M. (2019). MDM2-Recruiting PROTAC Offers Superior, Synergistic Antiproliferative Activity via Simultaneous Degradation of BRD4 and Stabilization of p53. Cancer Res *79*, 251-262.

48. Hodi, F.S., O'Day, S.J., McDermott, D.F., Weber, R.W., Sosman, J.A., Haanen, J.B., Gonzalez, R., Robert, C., Schadendorf, D., Hassel, J.C.*, et al.* (2010). Improved survival with ipilimumab in patients with metastatic melanoma. N Engl J Med *363*, 711-723.

49. Hosoe, S., Brauch, H., Latif, F., Glenn, G., Daniel, L., Bale, S., Choyke, P., Gorin, M., Oldfield, E., Berman, A.*, et al.* (1990). Localization of the von Hippel-Lindau disease gene to a small region of chromosome 3. Genomics *8*, 634-640.

50. Huang, D.T., Paydar, A., Zhuang, M., Waddell, M.B., Holton, J.M., and Schulman, B.A. (2005). Structural basis for recruitment of Ubc12 by an E2 binding domain in NEDD8's E1. Mol Cell *17*, 341-350.

51. Huang, X., and Dixit, V.M. (2016). Drugging the undruggables: exploring the ubiquitin system for drug development. Cell Res *26*, 484-498.

52. Iconomou, M., and Saunders, D.N. (2016). Systematic approaches to identify E3 ligase substrates. Biochem J *473*, 4083-4101.

53. Kaelin, W.G., Jr. (2007). The von Hippel-Lindau tumor suppressor protein and clear cell renal carcinoma. Clin Cancer Res *13*, 680s-684s.

54. Kanehisa, M., Furumichi, M., Tanabe, M., Sato, Y., and Morishima, K. (2017). KEGG: new perspectives on genomes, pathways, diseases and drugs. Nucleic Acids Res *45*, D353-D361.

55. Kaplan, D.H., Shankaran, V., Dighe, A.S., Stockert, E., Aguet, M., Old, L.J., and Schreiber, R.D. (1998). Demonstration of an interferon gamma-dependent tumor

surveillance system in immunocompetent mice. Proc Natl Acad Sci U S A *95*, 7556-7561.

56. Karaman, M.W., Herrgard, S., Treiber, D.K., Gallant, P., Atteridge, C.E., Campbell, B.T., Chan, K.W., Ciceri, P., Davis, M.I., Edeen, P.T.*, et al.* (2008). A quantitative analysis of kinase inhibitor selectivity. Nat Biotechnol *26*, 127-132.

57. Kim, W., Bennett, E.J., Huttlin, E.L., Guo, A., Li, J., Possemato, A., Sowa, M.E., Rad, R., Rush, J., Comb, M.J.*, et al.* (2011). Systematic and quantitative assessment of the ubiquitin-modified proteome. Mol Cell *44*, 325-340.

58. Klaeger, S., Heinzlmeir, S., Wilhelm, M., Polzer, H., Vick, B., Koenig, P.A., Reinecke, M., Ruprecht, B., Petzoldt, S., Meng, C.*, et al.* (2017). The target landscape of clinical kinase drugs. Science *358*.

59. Kopanja, D., Roy, N., Stoyanova, T., Hess, R.A., Bagchi, S., and Raychaudhuri, P. (2011). Cul4A is essential for spermatogenesis and male fertility. Dev Biol *352*, 278-287.

60. Koren, I., Timms, R.T., Kula, T., Xu, Q., Li, M.Z., and Elledge, S.J. (2018). The Eukaryotic Proteome Is Shaped by E3 Ubiquitin Ligases Targeting C-Terminal Degrons. Cell *173*, 1622-1635 e1614.

61. Kronke, J., Fink, E.C., Hollenbach, P.W., MacBeth, K.J., Hurst, S.N., Udeshi, N.D., Chamberlain, P.P., Mani, D.R., Man, H.W., Gandhi, A.K.*, et al.* (2015). Lenalidomide induces ubiquitination and degradation of CK1alpha in del(5q) MDS. Nature *523*, 183-188.

62. Kronke, J., Udeshi, N.D., Narla, A., Grauman, P., Hurst, S.N., McConkey, M., Svinkina, T., Heckl, D., Comer, E., Li, X.*, et al.* (2014). Lenalidomide causes selective degradation of IKZF1 and IKZF3 in multiple myeloma cells. Science *343*, 301-305.

63. Krummel, M.F., and Allison, J.P. (1995). CD28 and CTLA-4 have opposing effects on the response of T cells to stimulation. J Exp Med *182*, 459-465.

64. Lai, A.C., and Crews, C.M. (2017). Induced protein degradation: an emerging drug discovery paradigm. Nat Rev Drug Discov *16*, 101-114.

65. Lai, A.C., Toure, M., Hellerschmied, D., Salami, J., Jaime-Figueroa, S., Ko, E., Hines, J., and Crews, C.M. (2016). Modular PROTAC Design for the Degradation of Oncogenic BCR-ABL. Angew Chem Int Ed Engl *55*, 807-810.

66. Langmead, B., and Salzberg, S.L. (2012). Fast gapped-read alignment with Bowtie 2. Nat Methods *9*, 357-359.

67. Leach, D.R., Krummel, M.F., and Allison, J.P. (1996). Enhancement of antitumor immunity by CTLA-4 blockade. Science *271*, 1734-1736.

68. Lee, S.C., and Abdel-Wahab, O. (2016). Therapeutic targeting of splicing in cancer. Nat Med *22*, 976-986.

69. Lerman, M.I., Latif, F., Glenn, G.M., Daniel, L.N., Brauch, H., Hosoe, S., Hampsch, K., Delisio, J., Orcutt, M.L., McBride, O.W.*, et al.* (1991). Isolation and regional localization of a large collection (2,000) of single-copy DNA fragments on human chromosome 3 for mapping and cloning tumor suppressor genes. Hum Genet *86*, 567-577.

70. Levkowitz, G., Waterman, H., Ettenberg, S.A., Katz, M., Tsygankov, A.Y., Alroy, I., Lavi, S., Iwai, K., Reiss, Y., Ciechanover, A.*, et al.* (1999). Ubiquitin ligase activity and tyrosine phosphorylation underlie suppression of growth factor signaling by c-Cbl/Sli-1. Mol Cell *4*, 1029-1040.

71. Levy, A.P., Levy, N.S., Iliopoulos, O., Jiang, C., Kaplin, W.G., Jr., and Goldberg, M.A. (1997). Regulation of vascular endothelial growth factor by hypoxia and its modulation by the von Hippel-Lindau tumor suppressor gene. Kidney Int *51*, 575-578.

72. Lin, C.Y., Chen, C.Y., Yu, C.H., Yu, I.S., Lin, S.R., Wu, J.T., Lin, Y.H., Kuo, P.L., Wu, J.C., and Lin, S.W. (2016). Human X-linked Intellectual Disability Factor CUL4B Is Required for Post-meiotic Sperm Development and Male Fertility. Sci Rep *6*, 20227.

73. Lu, G., Middleton, R.E., Sun, H., Naniong, M., Ott, C.J., Mitsiades, C.S., Wong, K.K., Bradner, J.E., and Kaelin, W.G., Jr. (2014). The myeloma drug lenalidomide promotes the cereblon-dependent destruction of Ikaros proteins. Science *343*, 305-309.

74. Lugo, T.G., Pendergast, A.M., Muller, A.J., and Witte, O.N. (1990). Tyrosine kinase activity and transformation potency of bcr-abl oncogene products. Science *247*, 1079-1082.

75. Lunde, B.M., Moore, C., and Varani, G. (2007). RNA-binding proteins: modular design for efficient function. Nat Rev Mol Cell Biol *8*, 479-490.

76. Lyapina, S., Cope, G., Shevchenko, A., Serino, G., Tsuge, T., Zhou, C., Wolf, D.A., Wei, N., Shevchenko, A., and Deshaies, R.J. (2001). Promotion of NEDD-CUL1 conjugate cleavage by COP9 signalosome. Science *292*, 1382-1385.

77. Matyskiela, M.E., Clayton, T., Zheng, X., Mayne, C., Tran, E., Carpenter, A., Pagarigan, B., McDonald, J., Rolfe, M., Hamann, L.G.*, et al.* (2020). Crystal structure of the SALL4-pomalidomide-cereblon-DDB1 complex. Nat Struct Mol Biol.

78. Matyskiela, M.E., Couto, S., Zheng, X., Lu, G., Hui, J., Stamp, K., Drew, C., Ren, Y., Wang, M., Carpenter, A.*, et al.* (2018). SALL4 mediates teratogenicity as a thalidomide-dependent cereblon substrate. Nat Chem Biol *14*, 981-987.

79. Matyskiela, M.E., Lu, G., Ito, T., Pagarigan, B., Lu, C.C., Miller, K., Fang, W., Wang, N.Y., Nguyen, D., Houston, J.*, et al.* (2016). A novel cereblon modulator recruits GSPT1 to the CRL4(CRBN) ubiquitin ligase. Nature *535*, 252-257.

80. Maxwell, P.H., Wiesener, M.S., Chang, G.W., Clifford, S.C., Vaux, E.C., Cockman, M.E., Wykoff, C.C., Pugh, C.W., Maher, E.R., and Ratcliffe, P.J. (1999). The tumour suppressor protein VHL targets hypoxia-inducible factors for oxygen-dependent proteolysis. Nature *399*, 271-275.

81. Merbl, Y., and Kirschner, M.W. (2009). Large-scale detection of ubiquitination substrates using cell extracts and protein microarrays. Proc Natl Acad Sci U S A *106*, 2543-2548.

82. Merbl, Y., Refour, P., Patel, H., Springer, M., and Kirschner, M.W. (2013). Profiling of ubiquitin-like modifications reveals features of mitotic control. Cell *152*, 1160-1172.

83. Miura, H., Quadros, R.M., Gurumurthy, C.B., and Ohtsuka, M. (2018). Easi-CRISPR for creating knock-in and conditional knockout mouse models using long ssDNA donors. Nat Protoc *13*, 195-215.

84. Mullard, A. (2019a). Arvinas's PROTACs pass first safety and PK analysis. Nat Rev Drug Discov *18*, 895.

85. Mullard, A. (2019b). First targeted protein degrader hits the clinic. Nat Rev Drug Discov.

86. Neklesa, T.K., Winkler, J.D., and Crews, C.M. (2017). Targeted protein degradation by PROTACs. Pharmacol Ther *174*, 138-144.

87. Nguyen, A.T., Prado, M.A., Schmidt, P.J., Sendamarai, A.K., Wilson-Grady, J.T., Min, M., Campagna, D.R., Tian, G., Shi, Y., Dederer, V.*, et al.* (2017). UBE2O remodels the proteome during terminal erythroid differentiation. Science *357*.

88. Nguyen, T.V., Lee, J.E., Sweredoski, M.J., Yang, S.J., Jeon, S.J., Harrison, J.S., Yim, J.H., Lee, S.G., Handa, H., Kuhlman, B.*, et al.* (2016). Glutamine Triggers Acetylation-Dependent Degradation of Glutamine Synthetase via the Thalidomide Receptor Cereblon. Mol Cell *61*, 809-820.

89. O'Connor, H.F., Lyon, N., Leung, J.W., Agarwal, P., Swaim, C.D., Miller, K.M., and Huibregtse, J.M. (2015). Ubiquitin-Activated Interaction Traps (UBAITs) identify E3 ligase binding partners. EMBO Rep *16*, 1699-1712.

90. O'Connor, H.F., Swaim, C.D., Canadeo, L.A., and Huibregtse, J.M. (2018). Ubiquitin-Activated Interaction Traps (UBAITs): Tools for Capturing Protein-Protein Interactions. Methods Mol Biol *1844*, 85-100.

91. Ohh, M., Park, C.W., Ivan, M., Hoffman, M.A., Kim, T.Y., Huang, L.E., Pavletich, N., Chau, V., and Kaelin, W.G. (2000). Ubiquitination of hypoxia-inducible factor requires direct binding to the beta-domain of the von Hippel-Lindau protein. Nat Cell Biol *2*, 423-427.

92. Overington, J.P., Al-Lazikani, B., and Hopkins, A.L. (2006). How many drug targets are there? Nat Rev Drug Discov *5*, 993-996.

93. Owa, T., Yoshino, H., Okauchi, T., Yoshimatsu, K., Ozawa, Y., Sugi, N.H., Nagasu, T., Koyanagi, N., and Kitoh, K. (1999). Discovery of novel antitumor sulfonamides targeting G1 phase of the cell cycle. J Med Chem *42*, 3789-3799.

94. Ozawa, Y., Sugi, N.H., Nagasu, T., Owa, T., Watanabe, T., Koyanagi, N., Yoshino, H., Kitoh, K., and Yoshimatsu, K. (2001). E7070, a novel sulphonamide agent with potent antitumour activity in vitro and in vivo. Eur J Cancer *37*, 2275-2282.

95. Paiva, S.L., and Crews, C.M. (2019). Targeted protein degradation: elements of PROTAC design. Curr Opin Chem Biol *50*, 111-119.

96. Patel, R.K., and Jain, M. (2012). NGS QC Toolkit: a toolkit for quality control of next generation sequencing data. PLoS One *7*, e30619.

97. Peng, B., Hayes, M., Resta, D., Racine-Poon, A., Druker, B.J., Talpaz, M., Sawyers, C.L., Rosamilia, M., Ford, J., Lloyd, P.*, et al.* (2004). Pharmacokinetics

and pharmacodynamics of imatinib in a phase I trial with chronic myeloid leukemia patients. J Clin Oncol *22*, 935-942.

98. Peng, J., Schwartz, D., Elias, J.E., Thoreen, C.C., Cheng, D., Marsischky, G., Roelofs, J., Finley, D., and Gygi, S.P. (2003). A proteomics approach to understanding protein ubiquitination. Nat Biotechnol *21*, 921-926.

99. Pettersson, M., and Crews, C.M. (2019). PROteolysis TArgeting Chimeras (PROTACs) - Past, present and future. Drug Discov Today Technol *31*, 15-27.

100. Petzold, G., Fischer, E.S., and Thoma, N.H. (2016). Structural basis of lenalidomide-induced CK1alpha degradation by the CRL4(CRBN) ubiquitin ligase. Nature *532*, 127-130.

101. Quadros, R.M., Miura, H., Harms, D.W., Akatsuka, H., Sato, T., Aida, T., Redder, R., Richardson, G.P., Inagaki, Y., Sakai, D.*, et al.* (2017). Easi-CRISPR: a robust method for one-step generation of mice carrying conditional and insertion alleles using long ssDNA donors and CRISPR ribonucleoproteins. Genome Biol *18*, 92.

102. Rask-Andersen, M., Almen, M.S., and Schioth, H.B. (2011). Trends in the exploitation of novel drug targets. Nat Rev Drug Discov *10*, 579-590.

103. Ribas, A., Dummer, R., Puzanov, I., VanderWalde, A., Andtbacka, R.H.I., Michielin, O., Olszanski, A.J., Malvehy, J., Cebon, J., Fernandez, E.*, et al.* (2017). Oncolytic Virotherapy Promotes Intratumoral T Cell Infiltration and Improves Anti-PD-1 Immunotherapy. Cell *170*, 1109-1119 e1110.

104. Rodriguez-Gonzalez, A., Cyrus, K., Salcius, M., Kim, K., Crews, C.M., Deshaies, R.J., and Sakamoto, K.M. (2008). Targeting steroid hormone receptors for

ubiquitination and degradation in breast and prostate cancer. Oncogene *27*, 7201-7211.

105. Rowley, J.D. (1973). Letter: A new consistent chromosomal abnormality in chronic myelogenous leukaemia identified by quinacrine fluorescence and Giemsa staining. Nature *243*, 290-293.

106. Sakamoto, K.M., Kim, K.B., Kumagai, A., Mercurio, F., Crews, C.M., and Deshaies, R.J. (2001). Protacs: chimeric molecules that target proteins to the Skp1-Cullin-F box complex for ubiquitination and degradation. Proc Natl Acad Sci U S A *98*, 8554-8559.

107. Sakamoto, K.M., Kim, K.B., Verma, R., Ransick, A., Stein, B., Crews, C.M., and Deshaies, R.J. (2003). Development of Protacs to target cancer-promoting proteins for ubiquitination and degradation. Mol Cell Proteomics *2*, 1350-1358.

108. Salami, J., Alabi, S., Willard, R.R., Vitale, N.J., Wang, J., Dong, H., Jin, M., McDonnell, D.P., Crew, A.P., Neklesa, T.K.*, et al.* (2018). Androgen receptor degradation by the proteolysis-targeting chimera ARCC-4 outperforms enzalutamide in cellular models of prostate cancer drug resistance. Commun Biol *1*, 100.

109. Salami, J., and Crews, C.M. (2017). Waste disposal-An attractive strategy for cancer therapy. Science *355*, 1163-1167.

110. Santos, R., Ursu, O., Gaulton, A., Bento, A.P., Donadi, R.S., Bologa, C.G., Karlsson, A., Al-Lazikani, B., Hersey, A., Oprea, T.I.*, et al.* (2017). A comprehensive map of molecular drug targets. Nat Rev Drug Discov *16*, 19-34.

111. Schneekloth, J.S., Jr., Fonseca, F.N., Koldobskiy, M., Mandal, A., Deshaies, R., Sakamoto, K., and Crews, C.M. (2004). Chemical genetic control of protein levels: selective in vivo targeted degradation. J Am Chem Soc *126*, 3748-3754.

112. Scott, D.C., Sviderskiy, V.O., Monda, J.K., Lydeard, J.R., Cho, S.E., Harper, J.W., and Schulman, B.A. (2014). Structure of a RING E3 trapped in action reveals ligation mechanism for the ubiquitin-like protein NEDD8. Cell *157*, 1671-1684.

113. Seizinger, B.R., Rouleau, G.A., Ozelius, L.J., Lane, A.H., Farmer, G.E., Lamiell, J.M., Haines, J., Yuen, J.W., Collins, D., Majoor-Krakauer, D*., et al.* (1988). Von Hippel-Lindau disease maps to the region of chromosome 3 associated with renal cell carcinoma. Nature *332*, 268-269.

114. Shankaran, V., Ikeda, H., Bruce, A.T., White, J.M., Swanson, P.E., Old, L.J., and Schreiber, R.D. (2001). IFNgamma and lymphocytes prevent primary tumour development and shape tumour immunogenicity. Nature *410*, 1107-1111.

115. Sievers, Q.L., Petzold, G., Bunker, R.D., Renneville, A., Slabicki, M., Liddicoat, B.J., Abdulrahman, W., Mikkelsen, T., Ebert, B.L., and Thoma, N.H. (2018). Defining the human C2H2 zinc finger degrome targeted by thalidomide analogs through CRBN. Science *362*.

116. Silva, M.C., Ferguson, F.M., Cai, Q., Donovan, K.A., Nandi, G., Patnaik, D., Zhang, T., Huang, H.T., Lucente, D.E., Dickerson, B.C*., et al.* (2019). Targeted degradation of aberrant tau in frontotemporal dementia patient-derived neuronal cell models. Elife *8*.

117. Smith, B.E., Wang, S.L., Jaime-Figueroa, S., Harbin, A., Wang, J., Hamman, B.D., and Crews, C.M. (2019). Differential PROTAC substrate specificity dictated by orientation of recruited E3 ligase. Nat Commun *10*, 131.

118. Smyth, J.F., Aamdal, S., Awada, A., Dittrich, C., Caponigro, F., Schoffski, P., Gore, M., Lesimple, T., Djurasinovic, N., Baron, B.*, et al.* (2005). Phase II study of E7070 in patients with metastatic melanoma. Ann Oncol *16*, 158-161.

119. Talbot, D.C., von Pawel, J., Cattell, E., Yule, S.M., Johnston, C., Zandvliet, A.S., Huitema, A.D., Norbury, C.J., Ellis, P., Bosquee, L.*, et al.* (2007). A randomized phase II pharmacokinetic and pharmacodynamic study of indisulam as second-line therapy in patients with advanced non-small cell lung cancer. Clin Cancer Res *13*, 1816-1822.

120. Terret, C., Zanetta, S., Roche, H., Schellens, J.H., Faber, M.N., Wanders, J., Ravic, M., Droz, J.P., and Group, E.E.C.S. (2003). Phase I clinical and pharmacokinetic study of E7070, a novel sulfonamide given as a 5-day continuous infusion repeated every 3 weeks in patients with solid tumours. A study by the EORTC Early Clinical Study Group (ECSG). Eur J Cancer *39*, 1097-1104.

121. Thien, C.B., and Langdon, W.Y. (2001). Cbl: many adaptations to regulate protein tyrosine kinases. Nat Rev Mol Cell Biol *2*, 294-307.

122. Udeshi, N.D., Svinkina, T., Mertins, P., Kuhn, E., Mani, D.R., Qiao, J.W., and Carr, S.A. (2013). Refined preparation and use of anti-diglycine remnant (K-epsilon-GG) antibody enables routine quantification of 10,000s of ubiquitination sites in single proteomics experiments. Mol Cell Proteomics *12*, 825-831.

123. Uehara, T., Minoshima, Y., Sagane, K., Sugi, N.H., Mitsuhashi, K.O., Yamamoto, N., Kamiyama, H., Takahashi, K., Kotake, Y., Uesugi, M.*, et al.* (2017). Selective degradation of splicing factor CAPERalpha by anticancer sulfonamides. Nat Chem Biol *13*, 675-680.

124. Verma, R., Mohl, D., and Deshaies, R.J. (2020). Harnessing the Power of Proteolysis for Targeted Protein Inactivation. Mol Cell *77*, 446-460.

125. Walden, H., Podgorski, M.S., Huang, D.T., Miller, D.W., Howard, R.J., Minor, D.L., Jr., Holton, J.M., and Schulman, B.A. (2003). The structure of the APPBP1-UBA3-NEDD8-ATP complex reveals the basis for selective ubiquitin-like protein activation by an E1. Mol Cell *12*, 1427-1437.

126. Wang, E., Lu, S.X., Pastore, A., Chen, X., Imig, J., Chun-Wei Lee, S., Hockemeyer, K., Ghebrechristos, Y.E., Yoshimi, A., Inoue, D.*, et al.* (2019). Targeting an RNA-Binding Protein Network in Acute Myeloid Leukemia. Cancer Cell *35*, 369-384 e367.

127. Wang, Y., Liu, X., Zhou, L., Duong, D., Bhuripanyo, K., Zhao, B., Zhou, H., Liu, R., Bi, Y., Kiyokawa, H.*, et al.* (2017). Identifying the ubiquitination targets of E6AP by orthogonal ubiquitin transfer. Nat Commun *8*, 2232.

128. Woodhouse, N.J., and Sakati, N.A. (1983). A syndrome of hypogonadism, alopecia, diabetes mellitus, mental retardation, deafness, and ECG abnormalities. J Med Genet *20*, 216-219.

129. Xu, G., Paige, J.S., and Jaffrey, S.R. (2010). Global analysis of lysine ubiquitination by ubiquitin remnant immunoaffinity profiling. Nat Biotechnol *28*, 868-873.

130. Yamada, Y., Yamamoto, N., Shimoyama, T., Horiike, A., Fujisaka, Y., Takayama, K., Sakamoto, T., Nishioka, Y., Yasuda, S., and Tamura, T. (2005). Phase I pharmacokinetic and pharmacogenomic study of E7070 administered once every 21 days. Cancer Sci *96*, 721-728.

131. Yen, H.C., and Elledge, S.J. (2008). Identification of SCF ubiquitin ligase substrates by global protein stability profiling. Science *322*, 923-929.

132. Yen, H.C., Xu, Q., Chou, D.M., Zhao, Z., and Elledge, S.J. (2008). Global protein stability profiling in mammalian cells. Science *322*, 918-923.

133. Yin, Y., Lin, C., Kim, S.T., Roig, I., Chen, H., Liu, L., Veith, G.M., Jin, R.U., Keeney, S., Jasin, M.*, et al.* (2011). The E3 ubiquitin ligase Cullin 4A regulates meiotic progression in mouse spermatogenesis. Dev Biol *356*, 51-62.

134. Yin, Y., Liu, L., Yang, C., Lin, C., Veith, G.M., Wang, C., Sutovsky, P., Zhou, P., and Ma, L. (2016). Cell Autonomous and Nonautonomous Function of CUL4B in Mouse Spermatogenesis. J Biol Chem *291*, 6923-6935.

135. Zhang, C., Li, X., Adelmant, G., Dobbins, J., Geisen, C., Oser, M.G., Wucherpfenning, K.W., Marto, J.A., and Kaelin, W.G., Jr. (2015). Peptidic degron in EID1 is recognized by an SCF E3 ligase complex containing the orphan F-box protein FBXO21. Proc Natl Acad Sci U S A *112*, 15372-15377.

136. Zhao, B., Bhuripanyo, K., Zhang, K., Kiyokawa, H., Schindelin, H., and Yin, J. (2012). Orthogonal ubiquitin transfer through engineered E1-E2 cascades for protein ubiquitination. Chem Biol *19*, 1265-1277.